JOURNAL OF PROPULSION AND POWER
Vol. 25, No. 5, September–October 2009

Chemical Properties of Aircraft Engine Particulate Exhaust Emissions

Timothy B. Onasch,* John T. Jayne,† Scott Herndon,* Douglas R. Worsnop,† and Richard C. Miake-Lye†
Aerodyne Research, Inc., Billerica, Massachusetts 01821
I. Phil Mortimer‡
Johns Hopkins University, Baltimore, Maryland 21218
and
Bruce E. Anderson§
NASA Langley Research Center, Hampton, Virginia 23681

DOI: 10.2514/1.36371

The chemical properties of the particulate exhaust emissions from an in-use commercial aircraft engine were characterized in April 2004 as part of the Aircraft Particle Emissions Experiment. The test aircraft was the NASA DC-8 equipped with CFM56-2-C1 engines and the test matrix included 11 different engine throttle levels, three fuel compositions, and three sampling distances. The variations in particle emissions number, size, mass, and chemical composition were measured using a suite of instruments, including an aerosol mass spectrometer. The particle emissions were characterized by a trimodal size distribution. The largest mode was dominated by ambient accumulation mode particles mixed into the plume. The middle mode consisted of carbon soot with sulfate and organic coatings. The smallest mode was completely volatile and consisted of sulfate and organic components. The soot emission indices increased with power from 2–120 mg/kg fuel. The semivolatile components increased with distance and decreased with power from 33–5 mg/kg fuel. The sulfate emissions increased with distance and fuel sulfur content. The emissions under low power were dominated by organics, and the high-power conditions were dominated by soot. The CFM56 engine was less efficient at the low thrust levels typically used on the ground at an airport.

Introduction

EMISSIONS from aircraft are coming under increasing scrutiny. Although airplanes consume only a few percent of fossil fuel currently being used (8% of petroleum fuel products [1]), they may be significant local contributors of emissions to urban airsheds [2–5] and at altitudes [6–8]. With the continued growth of commercial air traffic, aviation emissions are anticipated to make an increasing contribution to pollution on local, regional, and global scales [9,10].

Particulate matter (PM) emissions have become the focus of much international attention as anthropogenic particles have been observed to impact human health and atmospheric processes locally and regionally as well as affecting global climate change [11,12]. Combustion-generated inorganic carbon soot particles directly absorb solar radiation, are implicated in climate forcing [13], and may indirectly affect cloud properties by activating into cloud droplets [14,15]. Specific open issues relating to aircraft particulate emissions include the quantification of particles that are emitted on the ground at airports and at altitude during flights and an understanding of the role of emitted aerosol precursors in particle nucleation, growth, and particle activation [10]. Relatively little is known about the chemical speciation and sources (e.g., contributions of lubricating oils to volatile particulate matter [10]) of the emissions of particles and aerosol precursor gases from aircraft engines, and so a number of recent studies [e.g., Atmospheric Effects of Aviation Project study, Experiment to Characterize Aircraft Volatile Aerosol and Trace Species Emissions (EXCAVATE), NASA/QinetiQ, PartEmis (measurement and predictions of the emission of aerosols and gaseous precursors from gas turbine engines), SULFUR 1–7] have been directed at improving understanding of these emissions and how they may contribute to particles in the atmosphere [16–20].

The Aircraft Particle Emissions Experiment (APEX) was conducted on 23–29 April 2004 at NASA Dryden Flight Research Center (DFRC) at Edwards Air Force Base, CA to characterize the particulate emissions of an in-use aircraft, the NASA DC-8 with four CFM56-2C1 engines [21]. With the airplane chocked in place on the ground, the inboard right engine (or engine #3) was sampled over a range of operating conditions from ground idle (4%) through full takeoff power (nominally 100%, actually 93%). The exhaust emissions were sampled at three distances downstream (1, 10, and 30 m) in an attempt to characterize the emissions near the engine exit plane (relevant to engine technology and certification testing) and downstream after the exhaust has diluted and cooled significantly (relevant to local airport environments). In addition to varying the engine power, three different aviation fuels (JP-8 fuel with moderate sulfur and aromatic contents, a high-sulfur JP-8 fuel, and a high-aromatic Jet-A fuel) were employed during APEX to begin exploring how fuel properties affect the resulting particle emissions.

Aerodyne Research, Inc. deployed its mobile laboratory in collaboration with multiple research groups including (not exclusive list) NASA, the University of Missouri–Rolla (UMR), and the U.S. Environmental Protection Agency. The Aerodyne mobile laboratory housed state-of-the-art instrumentation for measuring trace gas species and aerosol particle properties [22]. Gas phase measurements obtained in the mobile laboratory are reported elsewhere [23–25]. The physical and chemical properties of the particulate exhaust emissions (particle number, size, mass, and chemistry) were measured as a function of engine thrust, probe distance, and fuel type.

This paper focuses on the chemical composition and mass of the aircraft particulate exhaust measured during APEX. The particulate compositions were speciated using an aerosol mass spectrometer, filter-based refractory carbon soot absorption instruments, and a combination of heated and unheated scanning particle mobility sizers

Received 27 December 2007; revision received 5 January 2009; accepted for publication 31 January 2009.

*Principal Scientist, 45 Manning Road.
†Principal Scientist and Center Director, 45 Manning Road.
‡Manager, Mass Spectrometry Facility, Remsen B13.
§Senior Research Scientist, Mail Stop 483, 21 Langley Boulevard.

and condensation particle counters. Measurement results are provided as emission indices with units of mg/kg fuel for mass-based measurements and number/kg fuel for count-based measurements. This study focused on bringing chemical closure (mass-based accounting of all major chemical components) to the particulate exhaust emissions through the combination of the different particulate measurements.

Experimental Section

The Aerodyne mobile laboratory was outfitted with trace gas and particulate instrumentation. All onboard instruments drew air from the same sampling line inside the mobile laboratory and are depicted in Fig. 1. The gas phase measurements obtained in the mobile laboratory are reported elsewhere [23–25]. The particle measurements were conducted using the Aerodyne aerosol mass spectrometer (AMS) to characterize the size-resolved nonrefractory chemical composition and mass loadings, a condensation particle counter (CPC, TSI model 3022a) to measure the total particle concentration, and a modified multi-angle aerosol photometer (MAAP, Thermo Electron) to measure the aerosol absorption and derive black carbon soot mass concentrations. The particle instruments were operated downstream of a PM2.5 cyclone (URG-2000-30EN) to remove large particles. Additional particle instruments included in this analysis were operated by NASA and UMR and were located in nearby trailers [21,26].

Aircraft exhaust was sampled from three probes located 1, 10, and 30 m downstream in the aircraft engine exhaust flow. A sampling manifold distributed flow pulled from the downstream probes to the various particle-based research groups participating in APEX [21]. The sampling lines from the Aerodyne mobile laboratory were connected through ~6 m of sampling line to the distribution manifold located in another trailer. The manifold was operated at subambient pressures and was setup to provide ready access to any particular particle probe for a given engine condition. The manifold pressure was constant at ~650 torr when sampling from the 30 m probe under all engine power settings. Sampling from the 1 and 10 m probes, however, the manifold pressure changed dramatically (<500 to >700 torr) depending upon engine power and sample dilution ratio settings. Probes and associated sampling lines that were not being sampled were static with no flow. This fact may have resulted in some spurious measurements, specifically when switching from the 10 or 30 m probes to the 1 m probe, where PM may have collected in the forward facing probe tip through virtual impaction while no flow was being drawn. Whenever possible, suspected sampling artifacts (e.g., short-lived transient spikes in loadings observed during probe sampling changes) were discarded from the analysis.

Aerosol Mass Spectrometer

The Aerodyne aerosol mass spectrometer has been described in detail in the literature [27,28]. The AMS sampled aerosols into a high vacuum and focused the particles into a tight beam (<4 mm diam) using an aerodynamic lens. The focused particle beam exiting the lens was directed through a particle-sizing chamber and impacted on a 3.8-mm circular vaporizer held at 600°C. By mechanically modulating the particle beam with a chopper and using the particle time-of-flight (PTOF) between the chopper and the detector, the particle velocity and the vacuum aerodynamic diameter were obtained. The particle detection scheme consisted of a vaporizer that was coupled into the ionizer cage of a quadrupole mass spectrometer (MS). When the particles struck the vaporizer surface, the nonrefractory (semivolatile) components of particles flash vaporized. The vaporization plume was ionized using standard 70 eV electron impact ionization techniques and extracted into the mass spectrometer, which was scanned over a range of 1–300 atomic mass units. The AMS was operated during this study with a time-resolution of 30 s, alternating every 15 s between a PTOF mode (particle mass distributions as a function of size) and an MS mode (particle chemical speciation and mass loadings) [29].

Size and mass calibrations of the instrument were performed using polystyrene latex spheres and ammonium nitrate aerosol sources following established procedures [27,30]. The electron multiplier signals were calibrated at m/z (mass-to-charge ratio) 30 and 46 for nitrate (NO_3^+) and 15, 16, and 17 for ammonium (NH_4^+). The AMS analysis uses relative ionization efficiencies (relative to nitrate) measured in previous laboratory studies to quantify the chemical species present in aircraft exhaust (sulfates and organics). During this experiment, the AMS had a nitrate ionization efficiency of 6.9×10^{-6} ions/molecule and detection limits (3 times the standard deviation) of 0.024 and 0.26 $\mu g/m^3$, respectively, for sulfates and organics. Typical uncertainties for total nonrefractory inorganic and organic loadings are within 20%.

An additional uncertainty in the AMS measurements is the collection efficiency of the AMS. The aerodynamic inlet of the AMS efficiently transmits particles ranging in size from 50 to 700 nm in diameter [31]. Particles smaller than 70 nm and greater than 600 nm are lost due to diffusion and impaction during the sampling process. Essentially no particles smaller than about 30 nm or larger than 1 μm reach the detector. Within this size range, liquid particles are collected on the vaporizer with 100% efficiency, however, solid particles may bounce before full vaporization. Previous measurements on fractal-like soot particles indicate efficient collection (>90%) and detection in the AMS [32,33]. The likelihood of bounce depends on the phase and morphology of the particles and cannot be determined a priori. For this reason, the AMS mass loadings are reported in this paper as lower limits.

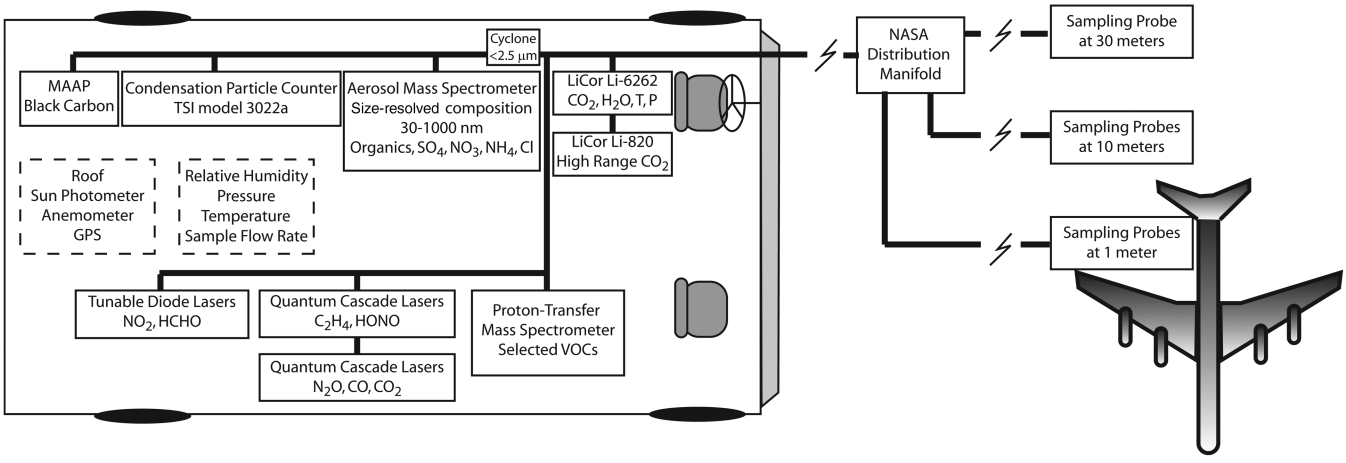

Fig. 1 Schematic of the Aerodyne mobile laboratory configuration deployed during APEX. The particle instruments were located on the left-hand side of the truck and isokinetically sampled aerosol behind a PM2.5 cyclone. All instruments in the mobile lab sampled from the same inlet line connected to the NASA distribution manifold.

Refractory Carbon Soot Measurements

Aerosol refractory carbon [interchangeably using refractory carbon and black carbon (BC) in paper] soot concentrations were derived with a Thermo Electron multi-angle aerosol photometer (Thermo Fisher), a particle soot absorption photometer (PSAP, Radiance Research), and a heated scanning mobility particle sizer (SMPS). A detailed description of the MAAP is provided in the literature [34,35]. The MAAP is a filter-based photometer that deposits aerosol onto a 2-cm^2 spot on a quartz fiber filter tape. A 630-nm wavelength light-emitting diode shines on the spot and multiple photodetectors measure the transmission and scattering/reflection of the light from the depositing aerosol layer and the underlying filter. A two-stream radiation transfer calculation is used to separate the absorption of the light by the aerosol layer from the scattering of light by the particles and filter matrix [35]. A narrow range of mass absorption coefficients, $\sigma_{abs} \sim 6.4$–$6.6\ m^2\ g^{-1}$, is reported to provide a decent fit between measured absorption coefficients and collocated particle mass measurements for commercially produced soot particles and urban particles containing refractory carbon soot collected at several sites [35]. A value of $\sigma_{abs} = 6.6\ m^2\ g^{-1}$ was used to calculate the instantaneous refractory carbon soot mass loading on the filter at a rate of 1 Hz. The MAAP was operated with a flow rate of 8 lpm. The precision of the MAAP for deriving refractory carbon soot mass loadings under these operating conditions was $\pm 2.4\ \mu g/m^3$.

The PSAP and the heated SMPS were operated by NASA Langley Research Center. The PSAP operates on similar techniques as the MAAP, however, it does not measure or correct for light scattered back from the filter, which must be done using postprocessing corrections [36].

Particle Counting and Sizing Instruments

The total aerosol number concentration was measured with several condensation particle counters (TSI models 3022a and 7061). The CPC supersaturates a sample flow with butanol vapor, causing submicron particles to grow in size into the supermicron size range where the particles are detected via individual light scattering pulses at low concentrations and via ensemble particle scattering at high concentrations. The 3022a CPC has a 50% cut size of 7 nm at atmospheric pressure, a response time of <10 s for 90% step change, and can sample particle concentrations up to $10^7\ cm^{-3}$. Two identical scanning mobility particle size instruments were also employed with TSI model 3025 CPCs to measure size distributions from 9–250-nm mobility diameter with a 60-s scan time. One SMPS sample stream was heated to over 300°C to remove nonrefractory compounds from the particles before size distribution measurements were conducted. The combination of the heated and unheated measurements allowed for the quantification of the total, refractory, and nonrefractory number- and volume-weighted size distributions.

Based on direct comparisons between the heated and unheated SMPS, the heated size distribution data have been corrected (15, 20, and 30% for the different probe sampling configurations at 1, 10, and 30 m, respectively) for a 15–30% particle transmission loss due to the presence of the heating element in the sampling line before the SMPS. The correction of the heated SMPS number distributions (carried through all subsequent calculations) was based on a direct comparison between the number distributions measured by the heated and unheated SMPS systems for the refractory soot mode (55–153 nm) under high engine power conditions (>60%). The fundamental test case was the 1-m probe measurements where there was no observed particle nucleation, and thus both SMPS systems should have measured the same total number of black carbon soot particles (even if there was a slight coating on them). The ratio of the heated/unheated size distributions was constant within experimental variations over this size range: the only particle mode measured in the heated SMPS. The 10 and 30-m probe measurements showed particle nucleation (shown later), but the nucleated particles did not grow into the 55–153-nm size range, and thus both SMPS instruments should have measured the same total number of soot particles and the heated SMPS was corrected accordingly. Interestingly, the ratio of heated/unheated size distributions in the 55–153-nm size range varied as a function of probe distance. Although the particle loss mechanisms responsible for these varying ratios are not currently known, the sampling line pressure (450–740 torr) and the particle number concentrations (>10×) did vary significantly as a function of probe distance and may have contributed to the variable losses via coagulation, thermophoresis, or diffusion processes.

Particle Effective Density Measurements

Size-dependent mass and volume measurements by the AMS (vacuum aerodynamic diameter d_{va}) and the SMPS (volume-weighted mobility diameter d_m) instruments can be used to determine a measure of the effective density of the exhaust particles. The relationship between the vacuum aerodynamic and mobility diameters is

$$d_{va} = \frac{\rho_p}{\rho_o} \times \frac{d_m}{\chi^2} \times \frac{C_c(d_{va}\chi\rho_o/\rho_p)}{C_c(d_m)} \quad (1)$$

where ρ and χ are particle density and dynamic shape factor, respectively, ρ_o is unit density (i.e., $1\ g/cm^3$), and C_c is the Cunningham, or slip, correction factor [32,37]. Equation (1) can be simplified to

$$d_{va} = \frac{\rho_{eff}}{\rho_o} d_m \quad (2)$$

where ρ_{eff} is the effective density ($\rho_{eff=}\rho_p/\chi^2 \times [C_c(d_{va}\chi\rho_o/\rho_p)/C_c(d_m)]$). The effective density defined here is related to ρ_{eff}^{III} as described in DeCarlo et al. [37] and differs by a constant factor (∼2.4) due to our use of the volume-weighted mobility diameter rather than the count mean diameter. The dynamic shape factor accounts for the effect of nonspherical shape on the particle drag force, equals one for spherical particles, and is almost always greater than one for nonspherical particles [38,39]. Thus, the vacuum aerodynamic diameter measured by the AMS was proportional to the volume-weighted mobility diameter measured by the SMPS instruments times the effective density of the particles. Simultaneous measurement of both mode diameters for a well-defined size distribution can provide information on the particles' effective density and particle shape.

To directly compare the AMS and SMPS results, the mass distributions measured by the AMS were corrected for varying pressure differences in the sampling line. The particle vacuum aerodynamic diameters were derived from particle time-of-flight (i.e., particle velocity) measurements inside the AMS. The velocity of the particles as they exited the aerodynamic lens inside the AMS was dependent upon the pressure inside the lens which, in turn, was directly related to the pressure inside the exhaust sampling lines. The sample pressure varied most significantly (450–740 torr) during 1-m probe sampling due to the large range of exhaust flow rates from the engine as a function of engine power and the large range of dilution flows required to control the dilution rates within the probe tip. Because of the difficulty of performing pressure-dependent size calibrations, this procedure was not done during the APEX mission, but rather later in the laboratory. The pressure-dependent size calibration was done on a different AMS than used during APEX; however, the laboratory-based instrument had the same aerodynamic lens design and chamber configuration as the instrument used during APEX. The corrections applied for this effect exhibited a maximum shift in vacuum aerodynamic diameter of 17 nm to larger sizes (∼20% change in mode diameter for 100-nm-diam particles) and a slight broadening of the distributions.

Emission Indices

Near-infrared absorption instruments (LiCor models 6262 and 840) were used to measure the gas phase CO_2 concentration in the sampled plume. The gas phase CO_2 concentration was used to relate the measured particulate mass loading to fuel-based particulate mass emission indices (EIs), with units of milligrams of particle mass per kilograms of fuel burned. Following the methodology described in

Herndon et al. [40] for a given exhaust component mass concentration X, the EI(X) was calculated by

$$\mathrm{EI}(X) = (\Delta X/\Delta \mathrm{CO_2}) \times \mathrm{EI}(\mathrm{CO_2}) \times M_{\mathrm{air}}/M_{\mathrm{CO_2}} \times (1/\rho_{\mathrm{air}}) \quad (3)$$

where $\Delta X/\Delta \mathrm{CO_2}$ was the emission ratio defined as the exhaust component mass concentration minus the background concentration divided by the difference in CO_2 concentrations over background, M_{air} was the molar mass of air, M_{CO2} was the molar mass of CO_2, and ρ_{air} was the density of air under the sampling conditions. As explained in the results section of this paper, ΔX has been replaced by X in this expression for AMS- and SMPS-derived EIs as the exhaust component mass concentrations were generated at different (smaller) particle sizes than any background aerosol (e.g., background aerosol mass was essentially zero at the relevant particle sizes). Equation (3) was based on the assumption that 100% of the carbon in the fuel was converted to CO_2. Corrections for CO and hydrocarbon emissions were not conducted as they were within experimental uncertainties for the measurements reported here. EI(CO_2) was measured based on fuel C/H compositions as 3160 g CO_2 per kg fuel for complete combustion of the fuels used during these tests (refer to next section).

Emission indices were also calculated for particle number-based emission indices (number per kg fuel) and derived volume-based emission indices (units of cubic centimeter per kilogram fuel, which is equivalent to grams per kilogram fuel for particles with unit density and spherical shape) using slightly modified versions of this formula. The reported EIs are noted as number-based (EI_n), mass-based (EI_m), and derived volume-based (EI_v) emission indices.

Sampling Conditions

The exhaust plume from the inboard right-side CFM56-2C1 engine on the NASA DC-8 aircraft was sampled on 23–29 April 2004 at NASA DFRC's aircraft facility located on Edwards Air Force Base. The key aspects of the particulate exhaust emissions characterized in this paper pertain to the size-dependent mass and chemical composition of the particles and the effects that engine operating conditions, sampling probe distance (e.g., plume downstream age), and aircraft fuel composition have on these particulate properties.

The aircraft was parked and chocked on a large concrete pad designed for engine run-up tests and held in place with onboard brakes during the tests. The ambient temperature varied from 19–36°C and the relative humidity varied from 5–21% during these measurements. Measurements were made behind the inboard CFM56-2-C1 engine on the right wing of the NASA DC-8-72 Airborne Laboratory Program aircraft using probes mounted at three different distances in the downstream exhaust flow (1, 10, and 30 m). Engine exhaust was characterized for 11 engine power conditions from ground idle (labeled 4% of maximum thrust) to takeoff power (labeled as 100% of maximum thrust; restricted to ~93% during tests) and three different fuel chemical compositions (a base fuel with moderate sulfur and aromatic contents, a high-sulfur fuel, and a high-aromatic fuel). Table 1 summarizes the different conditions varied during APEX.

Table 1 APEX sampling conditions

Variables	Conditions
Fuel type	JP-8 (BaseA), Jet-A (high aromatic), JP-8 (high sulfur)
Sampling distance	1 m (diluted), 10 m (diluted), 30 m (undiluted)
Engine thrust	4–100% of maximum rated thrust, including ICAO[a] standardized LTO[b] cycle (7% taxiing, 30% approach, 85% climbout, and 100% takeoff), 4% ground idle, and a few intermediate powers (5.5, 15, 40, 60, 65, 70%).

[a]International Civil Aviation Organization.
[b]Landing and takeoff.

The three different fuel compositions used during APEX to examine the effect of variable fuel composition (sulfur and aromatics) on the resulting particulate emissions were obtained two different ways. The base fuel was chosen to be the standard JP-8 fuel used at NASA DFRC and Edwards Air Force Base. Regional fuel suppliers were canvassed to obtain a fuel with a higher aromatic content (within aviation fuel specifications, but with higher aromatic content). A supplier of Jet-A fuel was found with a higher aromatic content than the base JP-8. The final fuel composition used, high-sulfur content, was the base JP-8 fuel doped with several gallons of a tertiary butyl disulfide additive. Table 2 shows the measured compositions of the fuels burned during APEX.

Sampling probes were located at downstream distances of 1, 10, and 30 m behind the engine exit plane. The sampling probes at 1 and 10 m consisted of a probe rake with multiple (six each) gas and particle probe tips located in a vertical line [21]. The 1-m probe was water cooled and had several extra gas, temperature, and pressure probes attached to the side of the rake. The particle sampling probe tips used at 1 and 10 m were designed to allow for dilution of the exhaust flow at the entrance of the probe tip to avoid water, sulfates, and volatile organic compound condensation inside the unheated sampling lines during rapid cooling of the hot exhaust. Compressed nitrogen was used to dilute the 1- and 10-m samples; the 1-m probe always required dilution, whereas the 10-m probe was sampled with and without added dilution. The dilution flows were monitored and controlled by NASA researchers based on measured CO_2 levels at the distribution manifold.

The 1- and 10-m probe tips were designed for near isokinetic sampling under most exhaust flow rates [21]. The #3 probe tip was chosen to be the main probe tip used at 1 m during the bulk of the APEX experiments based on the results from a mapping experiment [42]. Two (or more) nearby probe tips in the 10-m probe rake were combined for sampling to lower the pressure drop at the probe tips as the exhaust flow at 10 m was not as rapid and the dynamic pressure was lower. The 30-m probe had a different design than either the 1- or 10-m probes. The 30-m probe consisted of a single forward-facing tube with no dilution.

The particle sample transfer lines were unheated stainless steel tubes. The sample lines from the probes to the distribution manifold varied from 12.7-mm-i.d. tubing, ~20 m in length (1- and 10-m probes) to 48-mm-i.d. tubing , ~30 m in length (30-m probe). The residence times from sample probes to the distribution manifold varied from 6.2 s (1-m probe) to 2.7 s (30-m probe).

Particle Transmission Through Sampling Lines

A series of tests were conducted on the transmission of the sampling lines as a function of particle size (10–200 nm) for sodium chloride salt and diesel exhaust particle challenge aerosol. The experiments to assess transmission were done on site and using recreated sampling configurations at UMR [43]. Based on these tests, a best-estimate particle transmission curve for particles sampled by Aerodyne particle instruments starts at ~10% transmission at 10 nm and increases to an asymptote at 65–70% for particles larger than ~50 nm [42]. Transmission times through the sampling lines for all probes (1, 10, and 30 m) to the Aerodyne instruments was less than ~8 s. The effects of this particle transmission curve on the measured

Table 2 APEX fuel compositions [41]

Fuel type	Fuel label	Sulfur, ppmm	Aromatics, vol %	Hydrogen, wt %
JP-8	Base	383	17.6	13.69
JP-8	High sulfur	1595	17.3	13.67
Jet-A	High aromatic	530	21.6	13.7

number- and mass-based emission indices depends strongly on the distribution of number and mass as a function of particle size for the actual particles in the exhaust, as well as for the specific particle transmission functions of each instrument.

These particle transmission studies underscore the importance and difficulty in making quantitative measurements of aircraft engine particulate exhaust using extractive sampling techniques. The combination of these results suggests a potentially different particle transmission correction for each research group, due to the various sampling line lengths and configurations, especially for the smaller particles (<50 nm). Above 50 nm, the transmission efficiency is less dependent upon individual sampling line configurations. For the purposes of this paper on PM and chemical composition, the data have been compared and discussed without including particle transmission loss corrections. The potential effects these corrections may have on the data will be discussed within the context of the actual measurements, though are estimated to be less than a factor of 2 low in absolute magnitude for EI_m.

Results and Discussion

The chemical composition of the particulate exhaust is dependent upon the exhaust gas temperature as the plume exits the engine and mixes with cooler ambient air (or probe tip dilution N_2). The purpose of making three downstream extractive sampling probe measurements was an attempt to characterize the aircraft exhaust particulate chemistry and microphysics as a function of plume age and temperature. At 1 m behind the engine exit plane (typical distance for characterizing engines on test stands), the exhaust gas temperatures are hot (>300°C) and only refractory components are present in the particulate exhaust. The dry nitrogen dilution at the 1-m probe tip was designed to inhibit condensation of the nonrefractory (volatile and semivolatile) gaseous components in the sampling lines. At temperatures less than ~300°C (10 and 30 m downstream distances), nonrefractory gaseous components can nucleate new particles and condense on preexisting particles. The following discussion traces the changes in particle microphysics and chemistry with downstream distance, presents a chemical closure study from 30-m probe data, and concludes with observations on the chemistry of the nonrefractory particulate components.

Refractory Carbon Soot and 1-Meter Probe Distance

Under the specific sampling conditions 1 m downstream of the engine exit plane (i.e., high exhaust temperatures and added dilution inside the probe tip), only refractory components should exist in the particulate exhaust. During APEX, several instruments monitored these refractory PM components in real-time: heated (and, at 1-m probe distance, unheated) SMPS, CPC, MAAP, and PSAP. Figure 2a shows the average volume-based ($dEIv/d\log D$) emission indices as a function of particle diameter from the 1-m probe obtained with the unheated SMPS, Fig. 2d shows the average number-based EI_n, and Fig. 2e shows the average mass-based EI_m emission indices as a function of engine power setting from the 1, 10, and 30 m probes. The EI_n were derived from CPC measurements and the refractory EI_m were derived from MAAP, heated SMPS, and PSAP measurements. All of the data in Figs. 2a–2d, except for the EI_m plot (Fig. 2e), were obtained during times when the engine was burning high-aromatic fuel.

The $dEIv/d\log D$ distributions are monomodal and exhibit an increasing mode diameter (~40–100 nm) with engine power (7–100%). At 1 m, the average EI_n increased by a factor of approximately 10 (10^{14}–10^{15} particles per kg fuel) with increasing engine power (7–100%), at the same time that the particle EI_v mode diameter increased. The largest increase in EI_n occurred for engine power conditions above 80% of the maximum rated thrust. The increase in particle number and size increases the volume and mass loading of the particles as observed during the high engine power conditions in the $dEIv/d\log D$ size distributions and the refractory EI_m emission indices.

The MAAP, heated SMPS, and PSAP mass-based emission indices shown in Fig. 2e as a function of engine power are averaged over all probe distances and fuel types. Within the variation of measurements for a given instrument, the mass-based emission indices remained constant as a function of probe distance, indicating that the refractory carbon soot particles were being diluted at the same rate as the CO_2, as expected. Further, the refractory carbon soot

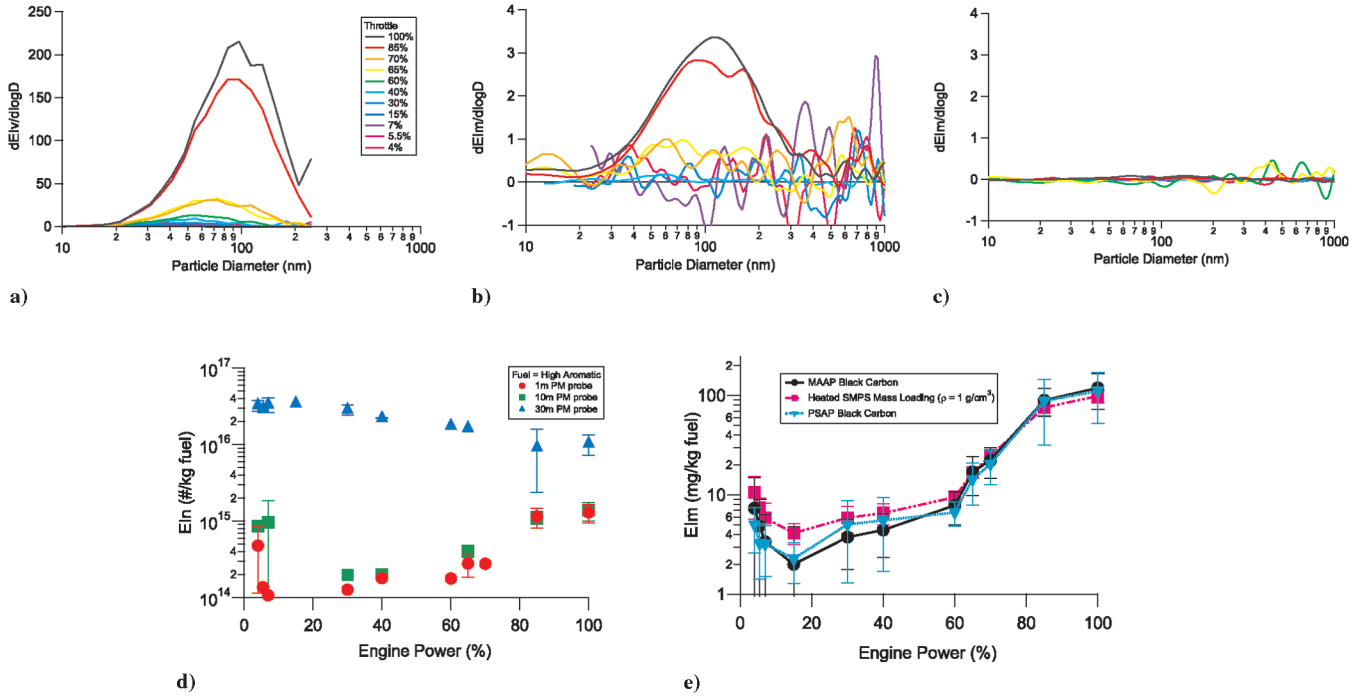

Fig. 2 Figures 2a–2c show the $dIE_v/d\log D$ and $dIE_m/d\log D$ (organic and sulfate, Figs. 2b and 2c, respectively) distributions obtained at the 1-m probe as a function of engine power. Figure 2d shows EI_n as a function of engine power for all three probes. All data shown in Figs. 2a–2d were obtained for the high-aromatic fuel case. Figure 2e shows the refractory carbon soot EI_m averaged over all sampling conditions (fuel type and probe locations) from the MAAP, heated SMPS, and PSAP.

EI_m did not vary significantly with fuel type combusted in the engine. The MAAP and PSAP measurements, both using filter-based absorption measurement techniques, were in very good agreement. The heated SMPS results appeared to be high at low engine powers and slightly low at high engine powers. These discrepancies may be due to the assumptions used in deriving the EI_v values from the SMPS number-based size distributions (spherical particles with unit density). The EI_m started at ~8 mg/kg fuel at the low engine powers (4–7%), dropped to 2–5 mg/kg fuel at intermediate engine powers (20–60%), and dramatically increased to ~100 mg/kg fuel at maximum rated thrust (100%).

The variability in the refractory carbon soot EI_m measurements shown in Fig. 2e may be due to several factors. At high engine powers, the largest factor is the fact that engine thrust settings (percent of maximum rated thrust) were chosen as the test designation during APEX. The thrust set point of the engine was calculated by the engine manufacturer, including the effects of ambient environmental conditions (e.g., temperature and wind speed), causing the engine combustion conditions (i.e., fuel flow, fan speed, etc.) used during APEX to vary with ambient conditions for a given nominal power setting [21]. The variation in engine combustion conditions explains most of the variability in the measured EI_m (Fig. 2e) at high engine power settings (refer to Fig. J-7 in the APEX report [42]). Thus, the fuel flow rate is a better independent variable to use compared with the nominal engine power settings that were chosen during APEX. Future experiments should use fuel flow rates as the designated power settings rather than estimated percent thrust levels. For the purpose of this paper, the nominal engine power settings will still be used as the primary independent variable, as this was chosen during the planning stages of APEX and makes direct comparisons between measurements simple. The large variations in refractory carbon soot EI_m at lower engine powers may be due in part to the signal-to-noise (S/N) levels of the MAAP and PSAP instruments near their detection limits. They may also be due to crosswinds that caused CO_2 and particle mass concentrations in the sampled exhaust plume to vary in time especially at the low-power setting (i.e., longer residence times between engine exit plane and sampling probe tip) and downstream probe distances.

Combining these refractory PM measurements (EI_n, EI_v, and EI_m) provides a straightforward picture of the particulate emissions of this CFM56-2C1 engine at 1 m behind the engine exit plane. At low engine powers, the soot particles generated in the combustors were small (~40 nm volume-weighted mobility diameter) and have a variable EI_n ranging from $1.0–5.0 \times 10^{14}$ particles per kg fuel and a EI_m of 8 mg/kg fuel. SMPS number-weighted size distributions (not shown) at the lowest engine powers appear to indicate possible nucleation in the 1-m probe causing the higher EI_n values observed for these conditions. At moderate engine powers (20–60% of maximum rated thrust), where the engine was operating close to the nominal thrust levels used during cruise at altitude, the soot exhaust particles increased in size to 60–70 nm (volume-weighted mobility diameter), whereas the EI_n were consistently below 3×10^{14} particles per kg fuel and the EI_m decreased to 2–5 mg/kg fuel. At high engine thrust levels (80–100%), a significant increase in soot generation was observed. The refractory carbon soot particles had a larger diameter (~100 nm volume-weighted mobility diameters), a higher EI_n (~1.5×10^{15} particles per kg fuel), and a EI_m of ~100 mg/kg fuel. Under all test conditions, the soot particles were present in a single lognormal mode.

The added dilution flow at the 1-m probe tip was expected to have prevented semivolatile material from condensing on the refractory carbon soot particles after sampling from the hot exhaust stream. However, a small amount of material was observed to condense on the soot particles. The nonrefractorydEIm/d log D distributions of organic and sulfate components as a function of particle vacuum aerodynamic diameter were obtained with the AMS (Figs. 2b and 2c). The AMS measured the nonrefractory compounds in and on the surface of particles. Thus, the AMS was sensitive to semivolatile material that may have condensed on the soot mode. Figure 3 shows an average over all fuel types of the total AMS mass measurements in units of milligram per kilogram fuel obtained as a function of engine power at the 1-m probe. The results suggest that the measured nonrefractory EI_m increased from 0.3 to 2 mg/kg fuel as the aircraft engine power increased from 4–100% thrust. The nonrefractory EI_m was dominated by organic composition. The sensitivity limit for the AMS measurements of organic components during APEX, described as 3 times the standard deviation of the signal when sampling filtered air, was 0.26 $\mu g/m^3$. Assuming a typical CO_2 concentration of 1500 ppmv in the sampled exhaust flow, the detection limit of the AMS for organic components was ~0.3 mg/kg fuel. This detection limit is shown in Fig. 3 as a dashed line. A comparison between this detection limit and the averaged AMS total nonrefractory EI_m for sampled exhaust at 1 m suggests that the results were at or below the detection limit for engine powers ranging from 7–30%. Above 30%, there is some indication of organic mass on the exhaust soot particles and there is measurable organic PM for engine powers greater than 80% thrust. This result, small compared with 30-m results, was not expected.

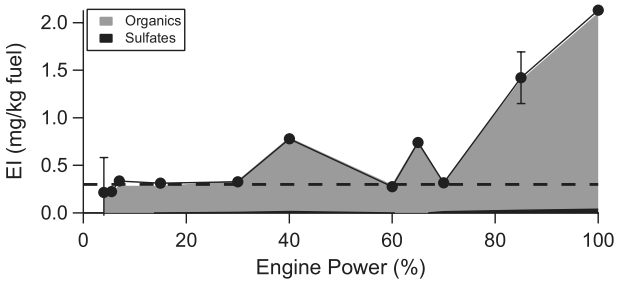

Fig. 3 Mass-based emission indices for the nonrefractory aerosol components measured by the AMS from the 1-m probe and plotted as a function of engine power. The black filled circles indicate the total nonrefractory EI, and the solid colors indicate that the majority of the measured mass was organic with an insignificant amount of sulfate. The dashed black line indicates a reasonable approximation of the detection limit of the AMS for the measurement of organic composition. See text for details.

The size-resolved EI_m for organic and sulfate particulate material shown in Figs. 2b and 2c, respectively, confirms that measurable nonrefractory particle mass was indeed organic and was only present during high engine throttle settings (>65%). Furthermore, this particle mass was present in a single size mode. The implication of these observations is that organic matter condensed onto the soot particles, likely during transit through the sampling lines.

As the temperatures of the core exhaust plume at the 1-m probe ranged from approximately 650–780 K and the plume age ranged from approximately 3–30 ms (calculated in our modeling work [44] based on Davidson and Wang's algorithms [45]), semivolatile (i.e., nonrefractory) compounds could not have condensed on the soot particles in the exhaust plume. Thus, the condensation must have occurred during the transit inside the sampling lines. This result indicates that the dilution with dry nitrogen (factor of 8–13) of the exhaust just inside the probe tip was not adequate at the high thrust levels to prevent condensation and some fraction of the semivolatile gaseous components condensed onto the soot particles. To further pursue this issue, future experiments should vary (increase) the sample dilution at the 1-m probe above the factor of 8–13 used during APEX.

The unexpected observation of the condensation of organic matter on the soot particles in the 1 m sample lines allowed the AMS to derive a vacuum aerodynamic diameter for the soot mode. Figure 4 compares the soot mobility EI_v distributions measured by the unheated SMPS instruments with the corrected vacuum aerodynamic organic particulate EI_m distribution observed by the AMS. The $dIE_m/d \log D$ and $dIE_v/d \log D$ data were plotted on separate y axes for normalization purposes, focusing on the diameter comparison rather than the magnitudes of the distributions. As both distributions are plotted on the same x axis, Eq. (2) indicates that the mode diameters should differ by a factor, the effective density (ρ_{eff}). Because the ratio of the mode diameters for the distributions are within 20% of each other, the obvious implication of Fig. 4 is that the effective

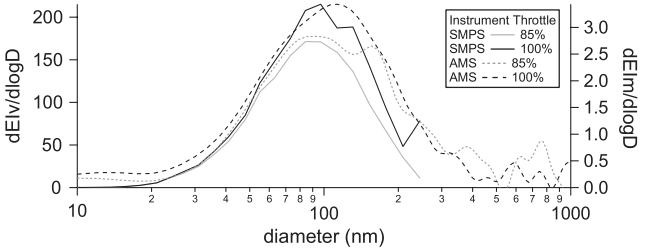

Fig. 4 Soot mode measured at 1 m by the SMPS instrument (right axis) and the AMS (left axis) for high-aromatic fuel at the indicated engine throttle conditions. The SMPS volume-weighted size distribution is plotted versus the particle mobility diameter, and the AMS mass distribution is plotted versus the particle vacuum aerodynamic diameter.

density of the soot mode generated at high engine throttle was approximately 1 g/cm^3.

Equation (1) can be used to derive a dynamic shape factor for the soot using the distributions' mode diameters. The material density of refractory carbon soot is typically in the range of 1.8–2.1 g/cm^3 [32]. The material density of the organic component may be assumed to be ∼0.9 g/cm^3 based on the densities of fuel and lubricating oil components. However, at these high engine powers, the mass of refractory carbon soot was much larger than the observed condensed organic particulate matter and thus the material density of the thinly coated soot particles was approximately 2 g/cm^3. Solving for the dynamic shape factor in Eq. (1), in a manner consistent with the iterative method described by Slowik et al. [32], yielded $\chi \sim 1.6$ for volume-weighted $d_m \sim 100$ nm soot particles. Thus, the refractory carbon soot particles generated by the CFM56-2-C1 engine were observed to be nonspherical.

As detailed in Slowik et al. [32], the dynamic shape factor of premixed laboratory flame and diesel engine generated refractory carbon soot particles is a function of the particle mobility diameter. In particular, Fig. 11 from Slowik et al. [32] shows derived dynamic shape factors for monodisperse fractal and spherical soot particles from flame and diesel soot as a function of particle mobility diameter. Figure 5 shows the current aircraft data compared with these previous soot particle observations. This exercise was done for several measurements of the soot mode from the 1- and 30-m probes for the high-aromatic fuel case. It turned out that the soot mode was only readily resolvable in the AMS under high engine power settings (85–100%), limiting the range in mobility diameter from this data set that can be used to only the largest soot sizes observed. The comparison in Fig. 5 indicates that the soot particles generated by the CFM56 aircraft engine were likely fractal in nature and not significantly different in morphology from soot generated by premixed laboratory flames and diesel engines. At the observed volume-weighted mobility diameters, the soot particles were not fluffy, large soot particles

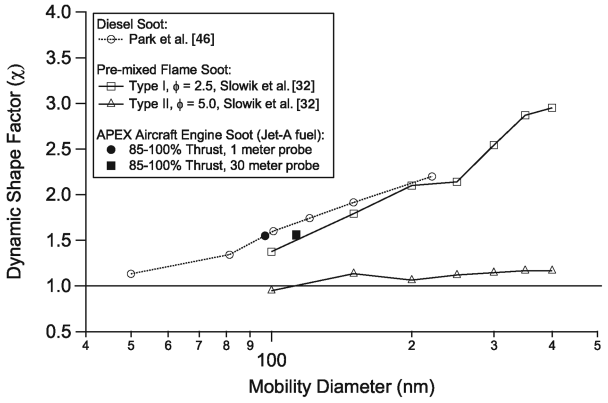

Fig. 5 The dynamic shape factor plotted versus the mobility diameter for the soot mode for the high-aromatic fuel case at 1 and 30 m. The results are compared to diesel soot morphology measurements obtained by Park et al. [46] and premixed laboratory flame soot obtained by Slowik et al. [32].

dramatically different from spherical, but were likely small, compact conglomerates consisting of a few (<20) primary particles with a shape factor differing modestly from that of a sphere ($\chi \sim 1.6$ compared with $\chi \sim 1.0$ for spherical particles).

The implications from these observations are that fractal-like, aircraft soot particles with a volume-weighted mobility diameter 40–100 nm have an effective density near unity (i.e., 1 g/cm^3). Interestingly, this result is similar to the effective densities observed for diesel truck emissions (1.2–0.8 g/cm^3 for particles ranging from 50–100 nm diameter) [46]. Thus, SMPS volume measurements can be converted to reasonably accurate mass measurements using an effective density of 1 g/cm^3, rather than the material density of black carbon of ∼2 g/cm^3. These results are used in this paper to convert SMPS black carbon volume to mass (e.g., refer to Fig. 2 comparison of MAAP, PSAP, and SMPS black carbon mass) and have been subsequently observed elsewhere [47]. The observed range in mobility diameters is much smaller for aircraft soot compared with the larger size ranges generated from diesel and premixed flames. Thus, although aircraft particles have similar fractal-like shapes, aircraft soot particle distributions are smaller and more compact (e.g., less fluffy) than typical combustion exhaust particulate distributions.

10-Meter Probe Distance

The 10-m probe represented the first downstream probe used during APEX and intercepted the exhaust plume at estimated temperatures ranging from 30–50°C higher than ambient with plume transit times from 30–200 ms [44]. Figures 6a–6c show the $dIE_v/d\log D$ and $dIE_m/d\log D$ size distributions and Figs. 6d and 6e show the distributions of EI_n and EI_m as a function of engine power for measurements obtained sampling through the 10-m probe for the base fuel case. The results for EI_n at 10 m were very similar to those observed at the 1-m probe for engine powers greater than 20%. This indicated that the particle number concentration was dominated by the soot mode at both the 1-m and 10-m probe distances. At low power (4–7%), the results from the 10-m probe indicated a consistently higher (10×) EI_n compared with the 1 m data. This difference, observed for all fuel types, indicated a new source of particles was present in the exhaust flow at low engine powers at the 10-m probe.

At 10-m distance, the exhaust plume had been cooled and diluted with a mixture of bypass flow and ambient air before being extracted into the sampling probe. A potential source of particles may have been gas-to-particle nucleation occurring at the 10-m probe distance at low engine powers. Although the $dIE_v/d\log D$ distributions in Fig. 6a did not register the presence of a nucleation mode, the number-weighted size distributions did show evidence for a nucleation mode (number-weighted size distributions available in the APEX report [21]). In fact, upon close examination, the nucleation mode was present during all engine power conditions at 10 m, and the SMPS and AMS recorded minor amounts of condensed non-refractory material in this mode. The particle number and volume of the nucleation mode decreased significantly at higher engine thrusts and thus was not readily observed in the averaged EI_n values shown in Fig. 6d. Although the distance of the 10-m probe was constant, the time the exhaust traveled to the probe, the extent of dilution with ambient air (and, subsequently, dilution air inside the probe tip), and the exhaust temperature varied with engine thrust. The velocity and temperature of the plume was dictated by the engine thrust level and, thus, the higher the engine power the younger the plume age (shorter transit time from engine exit to probe) and the hotter the exhaust before sampling at the 10-m probe. This change in plume age and temperature with engine power is a potential reason why new particle generation was a significant contributor to the total particle number only at low engine powers at the 10-m probe. Particle nucleation at low engine power settings also correlated with the largest gas phase concentrations of volatile organic compounds (VOCs) [24], suggesting that the slightly less-efficient operating conditions inside the combustors at low engine powers may have been the source for the condensable species participating in the particle nucleation and

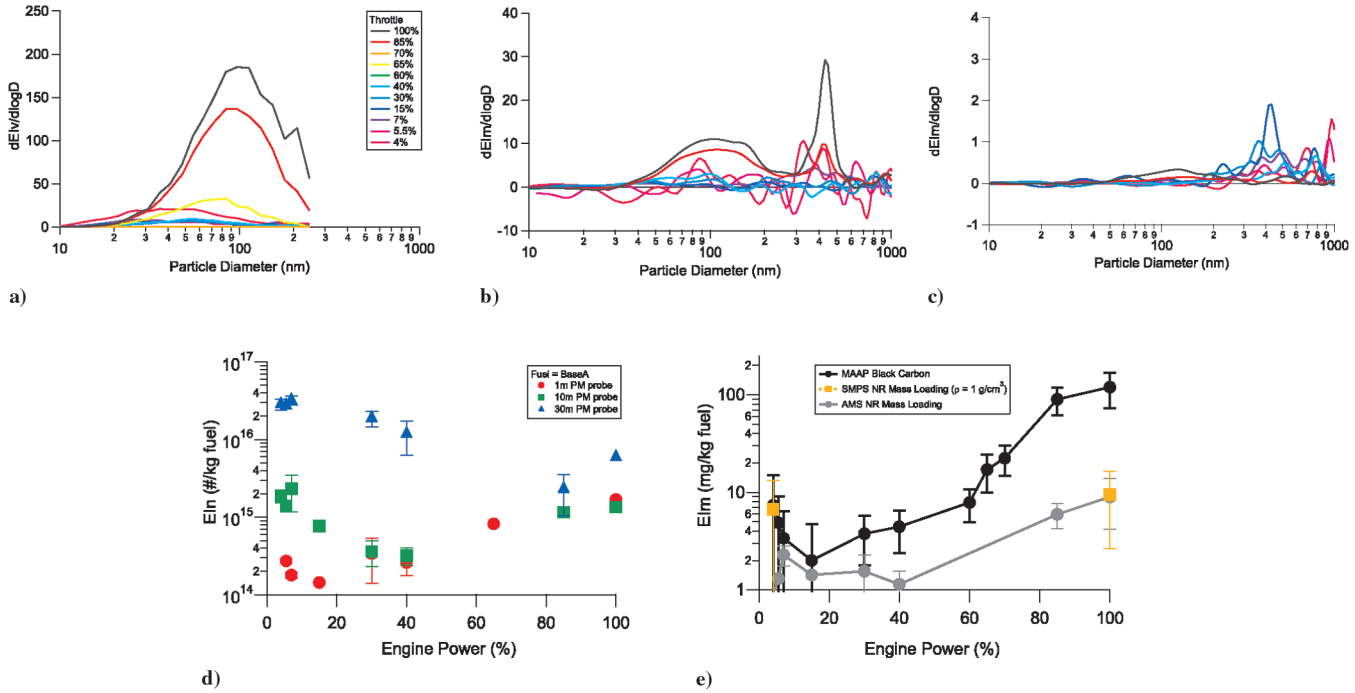

Fig. 6 Figures 6a–6c show the $dIE_v/d\log D$ and $dIE_m/d\log D$ (organic and sulfate, Figs. 6b and 6c, respectively) distributions obtained at the 10-m probe as a function of engine power. Figure 6d shows EI_n as a function of engine power for all three probes. All data shown in Figs. 6a–6d were obtained for the base fuel case. Figure 6e shows the MAAP black carbon EI_m averaged over all sampling conditions (fuel type and probe locations) and the SMPS and AMS nonrefractory EI_m for the base fuel case.

growth. It is not known if these particles were nucleating in the exhaust flow at 10 m or inside the diluted sampling lines similar to observations in the 1-m probe.

The SMPS $dIE_v/d\log D$ distributions (Fig. 6a) exhibit a similar result as obtained from the 1-m probe: a single soot mode that increased in mode size and total volume with engine power. The AMS $dIE_m/d\log D$ distributions (Figs. 6b and 6c) also showed similar results as obtained from the 1-m probe, including measurable organic and sulfate components condensed on the soot at high engine powers. The condensed particulate organic matter on the dominant soot mode was greater at 10 m compared to 1 m. There was also measurable organic and sulfate particulate matter in a mode located at approximately 300 nm vacuum aerodynamic diameter. This larger mode, not present in samples from the 1-m probe, was evidence for the entrainment of ambient particles into the exhaust stream before sampling into the 10-m probe. The large, narrow spike ~450 nm in the AMS organic and sulfate $dIE_m/d\log D$ distributions (Figs. 6b and 6c) is likely an artifact due to low-particle counting statistics and relatively large mass per particle at these larger sizes. Similar large spikes were observed by Laskin et al. [47] and described as aircraft emissions related, though it is unclear how they accounted for potential background aerosol entrainment in their samples.

Background Aerosol

When sampling at downstream locations, mixing of plume exhaust with background aerosol needs to be considered. Figures 7a and 7c show the background aerosol mass loadings and size-resolved chemical composition from midday on 21 April to the morning of 22 April 2004. This time period covered a morning and afternoon on two days when testing was delayed due to probe issues. Figures 7b and 7d show the large variations in chemical composition and mass loadings in time and their corresponding average size distributions. The average background organic and sulfate mass loadings were 0.3 and 0.4 $\mu g/m^3$, respectively; however, the concentrations varied by over a factor of 4 during this time period.

Despite the high variation in the background aerosol (which was not monitored while sampling aircraft exhaust), different sources of dilution air (ambient entrainment before sampling through the probe tip at 10 and 30 m and particle-free nitrogen inside the probe tip at 1 and 10 m), and the potential influence of the hot exhaust temperatures on the particle equilibria (e.g., entrained ambient aerosol could either have evaporated in the hotter exhaust plume and subsequently nucleated or recondensed onto the soot particles or acted as available particle surface area upon which gas phase species in the exhaust plume may have condensed as the exhaust cools), the background aerosol did not significantly complicate our ability to separate and quantify the exhaust particulate measurements. Based on limited observations, the background ambient particle mass resided in the large size accumulation mode and the exhaust particulate mass resided in the smaller soot and nucleated size modes. The ambient accumulation mode was measured to be internally mixed particles composed of organic, sulfate, nitrate, and ammonium with a vacuum aerodynamic mode size of ~350 nm. This was similar to the mode size observed in the exhaust sulfate and organic $dIE_m/d\log D$ distributions shown in Figs. 6b and 6c measured at the 10-m probe, indicating that ambient accumulation mode particles were mixing into the exhaust plume without significant volatilization (mode size changes). Furthermore, the mass loading measurements of organics and sulfate in the exhaust plumes ranged from 0.1–10 $\mu g/m^3$ for organics and 0–3 $\mu g/m^3$ for sulfates. Thus, even if the ambient particles were completely volatilized (but not oxidized) while passing through the engine or volatilized after mixing into the hotter exhaust plume, they could have only contributed a significant fraction (>10%) of the measured exhaust emissions during the low engine power conditions for this set of tests. Any potential mixing in of ambient black carbon soot would have had a negligible effect on the measured exhaust BC mass, as measured background refractory carbon soot mass concentration for these two days was low, approximately 0.3 $\mu g/m^3$, compared with the mass loading measurements during testing which ranged from 0.4–200 $\mu g/m^3$.

The entrained ambient aerosol mass was subtracted from the measured exhaust particulate mass before calculation of the EI_m values for the different test conditions by subtracting the large accumulation mode mass from the AMS mass distributions. The SMPS instruments used to sample the aircraft exhaust focused on the small particles being emitted from the aircraft and did not obtain information on the larger entrained ambient particle mode. Thus,

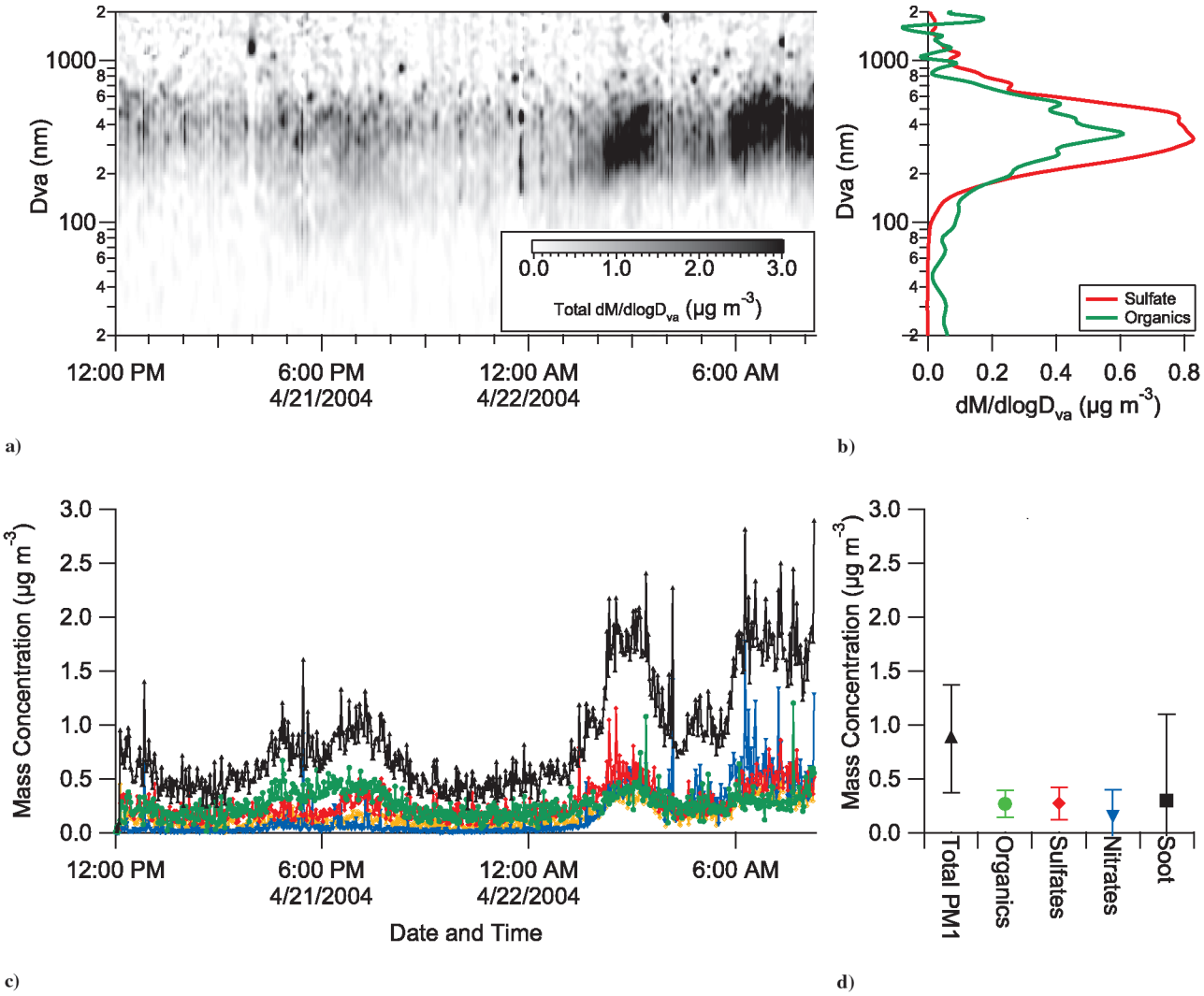

Fig. 7 Background nonrefractory aerosol chemical composition and size distributions measured by the AMS during 21–22 April 2004. Figure 7a shows the total nonrefractory size-resolved mass loadings, and Fig. 7b shows the average organic and sulfate mass distributions. Figure 7c shows the mass loadings as a function of time, and Fig. 7d shows the average mass concentrations for this time period.

there was no correction for ambient background loadings for the SMPS measurements. The average ambient mass loadings of refractory black carbon soot were subtracted from the MAAP and PSAP measurements, as indicated in Eq. (1).

An open issue with the methodology employed here is the uncertainty in how much of the nonrefractory exhaust particulate matter condensed on the ambient particles during dilution and entrainment. An example of this was the nonrefractory organic and sulfate components that were observed to condense on the soot mode at the 10-m probe (Figs. 6b and 6c). These same components likely also condensed on the ambient particles in the accumulation mode, however, we were unable to obtain sufficient information to quantify the amount condensed and prove that this had been the case.

30-Meter Probe Distance

The 30-m probe used during the APEX tests was designed to measure exhaust emissions properties downstream of the aircraft engines, representative of the exhaust plume after mixing with the local environment. At 30 m downstream, the engine exhaust flow had diluted and cooled significantly (dilution factors of >10 and temperatures just above ambient 25–50°C). The dilution and cooling of the exhaust plume caused the nonrefractory exhaust components to homogeneously nucleate new particles and to condense onto the nucleated particles and preexisting soot particles. The results from the 30-m probe showed a significant change in the microphysical properties of the particulate exhaust compared with 1- and 10-m locations. Figures 8a–8c show the $dIE_v/d\log D$ and $dIE_m/d\log D$ (organics and sulfates) distributions, and Fig. 8d shows the EI_n for measurements obtained sampling from the 30-m probe. The results in Fig. 8 contain data for the high-sulfur fuel.

The averaged EI_v distributions were plotted versus mobility diameter, whereas the averaged EI_m distributions were plotted versus vacuum mobility diameter. The $dIE_v/d\log D$ distributions (Fig. 8a) exhibited two volume-weighted modes: a ≤ 20 nm mode and a $\sim$100 nm mode. The $dIE_m/d\log D$ distributions (Figs. 8b and 8c) showed three mass modes: a ≤ 40 nm mode, a $\sim$100 nm mode, and a $\sim$400 nm mode. From the results obtained at 1- and 10-m probes, these modes were readily assigned as the nucleation/growth mode, the soot mode, and an entrained accumulation mode from ambient aerosols. The low counting statistics at the larger particles sizes caused the lower signal-to-noise levels in the accumulation mode measured by the AMS. The size distributions were dominated at low engine power settings by the smallest mode. The nucleation/growth mode diameter (volume-weighted mobility diameter) of the smaller mode was ≤ 20 nm at 7% idle and decreased slightly with increasing engine thrust. The soot mode only became significant at the highest engine powers. The accumulation mode was observed to be present in all of the $dIE_m/d\log D$ distributions, though the S/N was too low to clearly determine if significant organic or sulfate mass had condensed on the entrained ambient particles.

The EI_n results for all three probe distances are also shown in Fig. 8d. At the 30-m probe, the EI_n started at 3×10^{16} particles per kilogram fuel at low engine powers, approximately 2 orders of

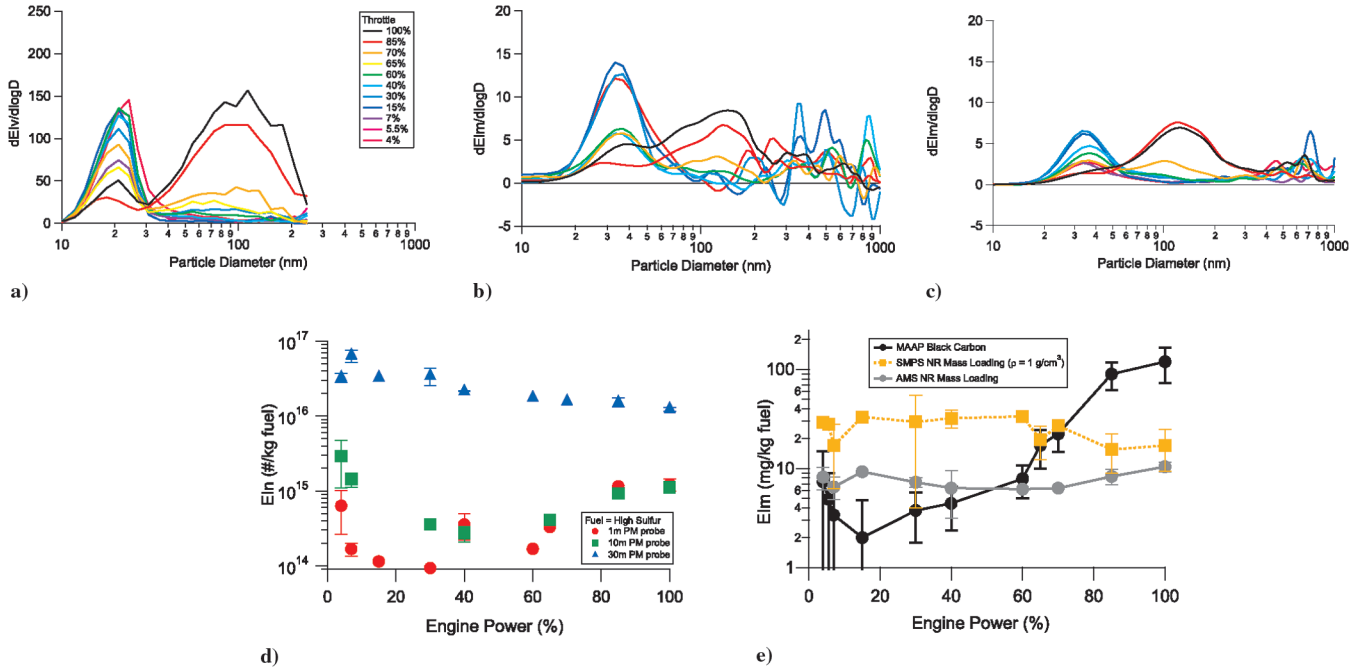

Fig. 8 Figures 8a–8c show the $dIE_v/d\log D$ and $dIE_m/d\log D$ (organic and sulfate, Figs. 8b and 8c, respectively) distributions obtained at the 30-m probe as a function of engine power. Figure 8d shows EI_n as a function of engine power for all three probes. All data shown in Fig. 8a–8d were obtained for the high-sulfur fuel case. Figure 8e shows the MAAP black carbon EI_m averaged over all sampling conditions (fuel type and probe locations) and the SMPS and AMS nonrefractory EI_m for the high-sulfur fuel case.

magnitude higher than the results at the 1-m probe, and slowly decreased to 1×10^{16} particles per kilogram fuel at 100% power. This dramatic increase in EI_n at 30 m downstream compared with the 1- and 10-m measurements was a result of gas-to-particle nucleation and condensational growth as the exhaust plume cooled through dilution with ambient air. The slight decrease in total particle number generated as a function of engine power was likely related to the increase in the soot particle number and size, such that the increased surface area of the refractory carbon soot particles decreased the supersaturation of the cooling vapors through heterogeneous condensation. Another potential explanation for the slight decrease in EI_n was the decreased plume age measured at the 30-m probe under high engine power conditions compared with low engine power conditions. The absolute magnitudes and observed decreasing trend in EI_n from idle to takeoff conditions were also observed by Herndon et al. [40] during in situ, advected plume measurements at several airports, suggesting that the former explanation is likely correct and suggesting that the 30-m probe results (i.e., extractive sampling techniques) may represent particle properties relevant to those in exhaust plumes after mixing into the local environment.

Observations of EI_n and EI_m during APEX (Figs. 2, 6, and 8) suggest that it requires at least ~30 m (~0.2 ms) to nucleate and condense significant nonrefractory mass to grow new particles to >10 nm in diameter. Although nucleation and condensation processes were observed at the 1- and 10-m probe distances (especially at the lower engine powers), they represented lower new particle number and mass concentrations than the 30-m probe results and are hypothesized to be artifacts of too little dilution or, perhaps, may represent the start of nucleation (10-m probe only). A complicating factor in understanding aircraft exhaust particle microphysics using extractive sampling techniques was the long time periods spent transiting the exhaust through sampling lines after entering the sampling line probe tips. For example, during sampling from the 30-m probe distance, the exhaust plume transited the 30 m in approximately 0.2–0.7 s (high to low engine power) and then spent >2.7 s in the sampling lines before detection in an instrument. Thus, the exhaust particles sampled during APEX at the 30-m probe may have been perturbed by the extractive sampling techniques employed, as observed in the 1- and 10-m cases. Independent of where condensation was occurring, the nonrefractory particulate exhaust number and mass were higher at the 30-m probe distance. Recent ground level modeling suggests that the nucleation and condensation of the nonrefractory components requires longer transition times (further distances downstream) than the 0.7 s (30-m probe), and thus must have occurred in the sampling lines during APEX [44]. Figure 8e shows the refractory (MAAP) and nonrefractory (SMPS and AMS) EI_m measured as a function of engine power. The chemical composition of the aircraft exhaust emissions calculated using the SMPS and MAAP measurements was composed of a significant fraction of nonrefractory mass at low engine powers, but only a minor component at high engine powers. The nonrefractory EI_m measured by the AMS was much less than the nonrefractory EI_m measured by the SMPS.

Chemical Closure Study

Figure 9 shows the chemical closure for the size-dependent EI_m measurements of the AMS (nonrefractory) and the EI_v measurements of the total SMPS (refractory plus nonrefractory) and the heated SMPS (refractory) at the 30-m probe distance for low (4%) and high (100%) engine power and for the base fuel case [fuel sulfur content (FSC) = 383 ppmm] and the high-sulfur fuel (FSC= 1595 ppmm). This comparison was done by plotting the $dIE_v/d\log D$ results versus the measured mobility diameter and the $dIE_m/d\log D$ results versus the measured vacuum aerodynamic diameter. For the soot mode, this method of comparison works rather well, as the difference in diameters is related to particle effective density [37], which was measured during this study to be ~1 g/cm^3. Thus, for the soot mode, the $dIE_v/d\log D$ and $dIE_m/d\log D$ measurements can be displayed on the same diameter scale. This method does not necessarily hold for the nucleation/growth mode, where the effective density is expected to be larger than unity. The difference between the EI_v and EI_m measurements for the nucleation/growth modes shown in Fig. 9 are understated ($EI_m > EI_v$) and the mode diameters are offset ($d_{va} > d_m$).

Three main observations are apparent in Fig. 9. The first is the presence of a significant amount of nonrefractory mass in the nucleation/growth mode measured by the SMPS in all cases except the high engine power, base fuel case. This result is in good agreement with the EI_n measurements in Figs. 2d, 6d, and 8d, indicating the presence of a significant number of nucleated particles at 30 m compared with the 1- and 10-m probe distances, with the

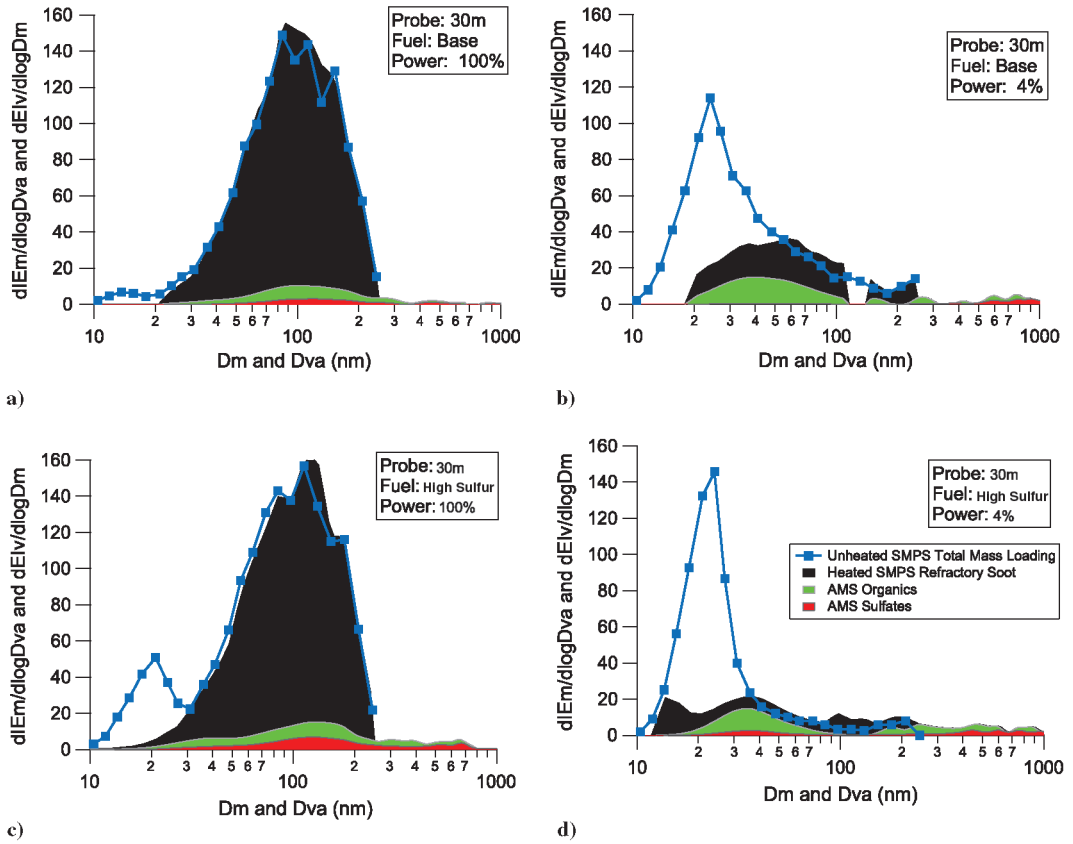

Fig. 9 Chemical composition of the aircraft engine exhaust for the base fuel case (Figs. 9a and 9b) and the high-sulfur fuel case (Fig. 9c and 9d). The solid black is the refractory carbon soot $\mathrm{d}IE_v/\mathrm{d}\log D$ measured by the heated SMPS, the solid red and green are the sulfate and organics $\mathrm{d}IE_m/\mathrm{d}\log D$ measured by the AMS, and the blue lines represent the unheated SMPS $\mathrm{d}IE_v/\mathrm{d}\log D$.

exception of the base fuel case at high engine powers (Fig. 6d) and the high nonrefractory EI_v and EI_m measured in the high-fuel sulfur case (Fig. 8). The second observation is that the magnitude of the EI_v in the nucleation/growth mode is not substantially different for the low- and high-fuel sulfur cases at low engine powers; however, the distribution of the EI_v as a function of size does differ for these two cases. The nucleation/growth mode for the base fuel case appears to be lower in magnitude and slightly larger in mode diameter, and the soot mode for the base fuel case appears to be higher in magnitude than the corresponding modes for the high-sulfur fuel case. This observation, taken in context of the lower EI_n measured at the 30-m probe for 4% engine power (compare Figs. 6d and 8d), is consistent with a similar amount of particulate mass of organic species distributed on fewer nucleated sulfate particles and the preexisting refractory carbon soot particles in the base fuel case compared to the higher number of sulfate nucleated particles in the high-sulfur case.

The third observation is that there is good agreement in chemical closure between the SMPS (total and refractory) and the AMS (nonrefractory) for the soot mode and poor agreement in chemical closure for the nucleation/growth mode (independent of the differences in the displayed EI and diameter scales). Thus, the missing nonrefractory mass measured by the AMS in Fig. 8e is due to the AMS not measuring a significant fraction of the nucleation/growth mode mass. The particle transmission into the AMS instrument at the small particle sizes caused a significant number of particles in the nucleation/growth mode to go undetected by the AMS. Recent laboratory tests indicated that the transmission curve for the AMS dropped below 100% around 100 nm and falls below 50% transmission below 60 nm in vacuum aerodynamic diameter [31]. Thus, as shown in Figs. 9b and 9d, the AMS cannot quantitatively measure the emission index from the nucleation/growth mode. In direct contrast, the soot mode lies completely within the high transmission efficiency range of the AMS, indicating that the AMS can quantitatively measure the EI_m of the nonrefractory components condensed on the soot mode.

Despite the lower size limit on the AMS sampling capabilities, the AMS can provide important information on the chemistry of both the soot and the nucleation/growth modes in the aircraft particulate exhaust emissions. The nonrefractory composition of the sampled aircraft particulate exhaust as measured by the AMS consisted of only organic and sulfate compounds in the nucleation/growth and soot modes. To better understand the chemistry of the exhaust particles, the AMS EI_m distribution data were fit using lognormal curves to deconvolve the fraction of particulate mass in each of the three modes.

Figure 10 shows the sulfate (Figs. 10a, 10c, and 10e) and organic (Figs. 10b, 10d, and 10f) EI_m as a function of engine power for the three types of fuels burned in the aircraft, measured at the 30-m probe. Figure 10e shows the sulfate and Fig. 10f shows the organic aerosol EI_m for the base fuel case. The lighter color indicates the mass measured in the soot mode, the darker color indicates the mass measured in the nucleation/growth mode, and the difference between the sum of these two curves and the total AMS (line in each plot) indicates the fraction of EI_m observed in the accumulation mode. Figures 10c and 10d show the high-aromatic fuel case and Figs. 10a and 10b show averages for the high-sulfur fuel case.

In all cases, the nonrefractory organic composition was the dominant component, with the exception of the high-sulfur fuel case where the measured nonrefractory composition was ~50% organic. The amount of sulfate and organic condensed on the soot mode increased with engine power. This indicated that the surface area of the soot mode was dramatically increasing with engine power and more gas phase components were condensing on the preexisting surface area. At low engine power conditions, the particulate exhaust appeared to be dominated by the nucleation/growth mode. The base and high-aromatic fuel cases exhibited very similar results for both the sulfate and organic components, compared with the high-sulfur fuel case. The high-sulfur fuel case showed more sulfate mass present in the EI_m distributions compared to the lower sulfur fuel cases. Interestingly, the high-sulfur fuel case appeared to also have more

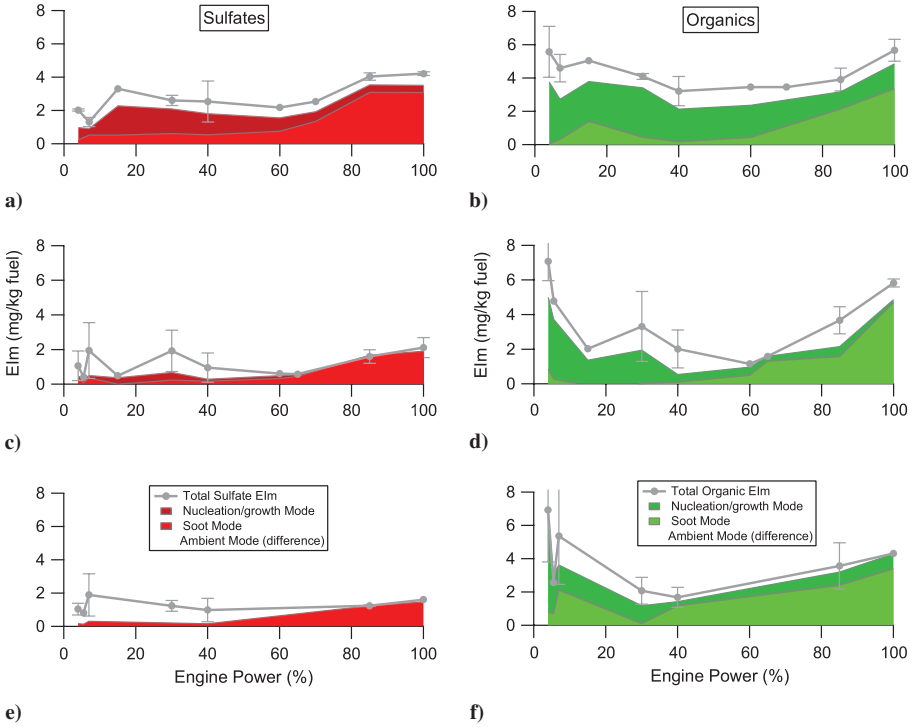

Fig. 10 Nonrefractory EI_m for sulfate and organic components in aircraft exhaust measured by the AMS. Figures 10a, 10c, and 10e show the sulfate EI_m as a function of engine power. Figures 10b, 10d, and 10f show the organic EI_m as a function of engine power. Figures 10a and 10b are averaged for the high-sulfur fuel case, Figs. 10c and 10d for the high-aromatic case, and Figs. 10e and 10f for the base fuel case. The lighter color represents the EI_m for the sulfate (Figs. 10a, 10c, and 10e) and organics (Figs. 10b, 10d, and 10f) condensed on the soot mode. The darker color represents the sulfate/organic measured in the nucleation/growth mode, and the gray lines are the sum of the EI_m for each species from the three modes (nucleation/growth, soot, and accumulation mode).

organic mass present in the nucleation/growth mode, whereas the base fuel case has more organic in the soot mode. The organic condensed on the soot mode was 3 ± 1 mg/kg fuel averaged over all fuel cases at high engine powers, indicating that the overall amount of organic matter that could condense on the particles was similar in all three fuel cases. The larger nucleation/growth mode organic EI_m observed under the high-sulfur fuel case is consistent with the SMPS EI_v distributions in Fig. 9, further indicating that the higher fuel sulfur content generates more nucleated particles at 30 m downstream, which influences the distribution of the condensed nonrefractory organic species.

The amount of sulfate present in the exhaust is presumed to be due to fuel sulfur content and postcombustor exhaust radical chemistry that converts SO_2 into SO_3 and H_2SO_4 molecules in the initial tens of meters downstream [48–50]. Some fraction of measured sulfate may have been due to entrained, vaporized, and recondensed sulfate from background air (See preceding section titled Background Aerosol). The H_2SO_4 molecules condensed onto preexisting aerosol surfaces or nucleated to form new particles directly from the gas phase as the exhaust cools after passing the engine exit plane. The SO_3 reacts rapidly with water after exiting the engine exit plane, converting more sulfur to H_2SO_4 downstream in the exhaust plume [51]. There was particulate sulfate in all size modes and under all experimental conditions with the exception of the base fuel case at low engine powers. It is assumed, but currently not known, that the generated gas phase sulfate molecules were the sole nucleating species and that the organic compounds could not nucleate new particles without sulfate.

With little observed difference in particulate sulfate EI_m as a function of engine power in the base and high-aromatic fuel cases, Fig. 11a shows the average low-sulfur fuel cases (base and high-aromatic fuel) nonrefractory EI_m compared with the volatile EI_m (i.e., $EI_v \times 1$ g/cm^3) measured by the SMPS (unheated–heated). The bottom solid bands of red and green are the sulfate and organic condensed on the soot mode, respectively, and the top red and green are the sulfate and organic in the nucleation/growth mode, respectively. The orange line is the integrated EI_v from the SMPS measurements for the volatile component assuming a density of unity. This number was derived by subtracting the heated SMPS measurements from the unheated SMPS measurements and represented the total particle volume of nonrefractory (300°C) material present on the aircraft exhaust over the measured mobility size range (10–240 nm). The total EI_m measured by the AMS agrees well with the estimated total EI_v measured by the SMPS at high engine powers for the low-sulfur fuel cases (Fig. 11a at high engine power). Furthermore, the AMS and SMPS distribution results indicated that most of the nonrefractory mass was condensed on the soot mode in these cases (Fig. 9a). It is unclear whether this is entirely due to the increase in soot surface area while the total organic EI_m decreased with engine power, or if the shorter times from engine exit plane to sampling probe (due to faster flow at higher powers) was also important. This result was further observed in the lower EI_n at higher engine powers at 30 m observed for the base fuel case (Fig. 6d), where the EI_n at high engine powers was similar to what was at 1 and 10 m from the soot particles.

At engine powers less than 70%, the nonrefractory EI_v measured by the SMPS instruments for the low-sulfur fuel cases was always greater than the total EI_m measured by the AMS (Fig. 11a). The AMS measured a small and increasing fraction (5–15%) of nonrefractory mass in the nucleation/growth mode with decreasing engine power, but the comparison indicated that the AMS was unable to measure most of the particulate mass in the nucleation/growth mode due to the small size of these particles. The AMS qualitatively observed more organic than sulfate material in the nucleation/growth mode as the engine power decreased. This final observation further supports the hypothesis that the high nonrefractory particulate mass at low engine powers is dominated by organic species that are distributed on the nucleated sulfate particles and the preexisting refractory soot particles.

Figure 11b also shows the AMS and SMPS measurements for nonrefractory particulate emission indices (EI_m and EI_v, respectively) for the high-sulfur fuel case. The comparison between the low- and high-fuel sulfur cases shows significant increase in the total nonrefractory EI_v measured by the SMPS for the high-fuel sulfur case compared with the low-fuel sulfur cases for all but the lowest engine powers (4%). Because the AMS should quantitatively

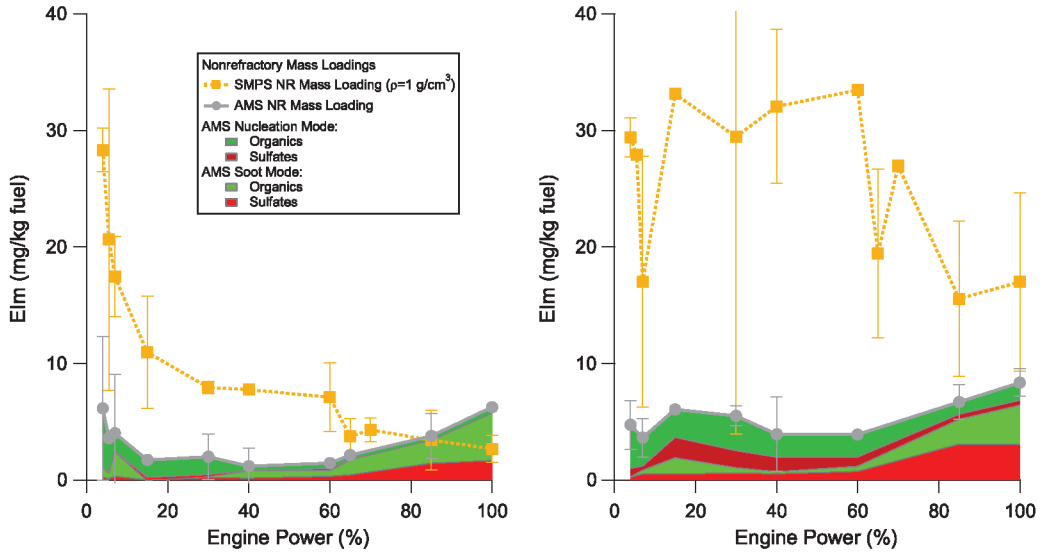

Fig. 11 A comparison between the AMS measured nonrefractory EI_m and the SMPS measured nonrefractory EI_v averaged for the a) low-sulfur fuel cases (base and high-aromatic fuels), and b) high-sulfur fuel case. The bottom two solid red and green are the sulfate and organics condensed on the soot mode, the top two solid red and green colors are the sulfate and organics measured by the AMS in the nucleation/growth mode, and the orange lines are the EI_v derived from the difference between the heated and unheated SMPS scans. The AMS measurements were stacked such that the total AMS EI_m measurements are the top of the solid bands.

measure the amount of condensed matter on the soot mode, the discrepancy between the AMS and SMPS measurements in the high-sulfur fuel implied that there was significantly more mass present in the nucleation/growth mode for all engine power conditions. This result is confirmed in the size distributions in Figs. 9c and 9d and the EI_n measurements in Fig. 8d. The organic EI_m measured by the AMS in the soot mode at high engine powers was similar for the low- and high-sulfur fuel cases; however, the sulfate mass on the soot mode was greater (by approximately a factor of 2). Thus, the dramatic increase in nonrefractory EI_v measured by the SMPS in the nucleation/growth mode particles may represent the extra sulfate generated from the high-sulfur content fuel. What is yet unexplained is why the nonrefractory EI_v measured by the SMPS is so similar in the low- and high-sulfur fuel cases at low engine powers, whereas the mid to high engine power results show such a difference. Two potential reasons for this observation are 1) the nucleated sulfate particles under low engine power conditions may not have grown enough to be fully measured by the SMPS instruments compared with higher engine power conditions, and 2) the conversion rate for oxidizing fuel sulfur into condensable sulfate may be reduced under low power conditions compared with higher engine power conditions.

Combining the nonrefractory and refractory EI_m for the low- and high-sulfur fuel cases, Figs. 12a and 12b show the chemical composition of the particulate exhaust emissions as a function of engine power for the low-sulfur fuel cases and high-sulfur fuel case, respectively. The nonrefractory EI_m shown in Figs. 12a and 12b are the same as shown in Figs. 11a and 11b, with the exception that the AMS measurements for components on the nucleation/growth mode and the soot mode are combined. The AMS measurements for sulfate and organics are shown in red and green, respectively, and the MAAP measurements of the refractory carbon soot are shown in black. These EI_m measurements were directly compared with the dotted blue line showing the EI_v measurements for the unheated SMPS measurements. The dotted orange line shows the nonrefractory fraction of the total SMPS EI_v. This measurement was derived from

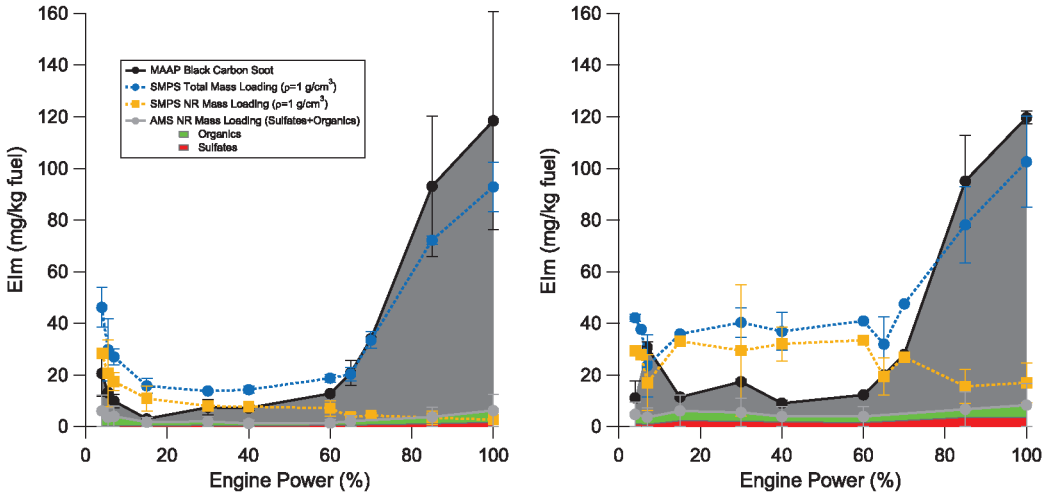

Fig. 12 Total chemical composition (refractory and nonrefractory) of the aircraft engine exhaust for the low-sulfur fuel cases and the high-sulfur fuel case are shown in Figs. 12a and 12b, respectively. The black represents the refractory carbon soot EI_m measured by the MAAP, the green and red represent the organics and sulfates measured by the AMS, the dotted blue lines represent the unheated SMPS EI_v, and the dotted orange lines represent the difference between the unheated and heated SMPS scans.

the difference between the unheated and heated (300°C) SMPS measurements. The dominant feature of Figs. 12a and 12b is the magnitude of the refractory carbon fraction at high engine powers (85–95%). The nonrefractory components (sulfate and organics) represent a significant fraction of the exhaust at low engine powers for both high- and low-sulfur fuel cases (50–80%). Thus, the nonrefractory mass fraction decreases as a function of increasing engine power.

Figures 9–12 show that nonrefractory exhaust from a CFM56-2-C1 engine burning fuel with high-sulfur content was strongly influenced by the increase in sulfate present. Under the high-sulfur fuel case (not typical of modern commercial fleet fuels), the refractory carbon soot still dominated at high engine powers, but the nonrefractory component was significant over the full engine power range and larger than the low-sulfur fuel case for all but the lowest engine powers. The additional nonrefractory particulate material was present in both the nucleation/growth and soot modes, though to a greater degree in the former, and contained a higher fraction of sulfate.

In the base and high-aromatic fuel cases, which represent more typical levels of fuel sulfur available to commercial aircraft, the nonrefractory aerosol composition appeared to be dominated by organic compounds and was significantly higher at the lower engine power conditions typically used for idling and taxiing around airports. The bulk of the nonrefractory components at low engine powers for the low-sulfur fuel cases was present in the nucleation/growth mode. The dramatic change in the nonrefractory to refractory chemical composition of the aircraft particulate exhaust has been previously observed using surface sensitive instrumentation (see Fig. 2 in [40]).

It is important to note that the particle loss experiments indicate that the magnitude of the mass (and number) in the nucleation/growth modes may be underrepresented by these uncorrected SMPS measurements by 40–90% [43], whereas the soot mode is likely well represented in number (and mass).

Nonrefractory Organics and Sulfates

The AMS mass spectral signals provide information on the chemical form of both sulfate and organic species and some information on the amount of nonrefractory mass generated in aircraft engine exhaust and condensed on the refractory carbon soot particles. The AMS underestimates the nonrefractory particulate mass in most cases studied here as the particle transmission efficiency of small particles (<70 nm diameter) into the AMS is limited and decreases with decreasing size [31]. In contrast, the AMS samples particles in the soot mode diameter range efficiently. Thus, in the specific case of the low-sulfur fuel cases under high engine powers, the AMS provides a reasonable limit (20% uncertainty with a potential bias due to collection efficiency issues, combined uncertainty of −20 and +120%) to the amount of nonrefractory mass generated in aircraft engine exhaust and condensed on the refractory carbon soot particles. This result still represents a lower limit due to the uncertainty in the AMS collection efficiency, though comparisons with SMPS EI_v appear to indicate high collection efficiencies for the soot particles, for example, soot mode chemical closure in Figs. 9 and 11.

The sulfate component, characterized via the AMS mass spectral fragmentation patterns, was observed to be acidic, though there was evidence for neutralization by ambient ammonia. The average sulfate measured by the AMS under high engine power conditions and condensed on the soot mode indicated that the amount of EI_m sulfate generated from the low-sulfur fuel cases was ∼1.5 mg/kg fuel. Under these conditions, the EI_n was measured to be 1×10^{15} particles/kg fuel (Fig. 6d). Thus, assuming uniform coverage of sulfate on each particle, this converts to ∼0.1 monolayer coverage of sulfate on the soot particles. Measurements using V-TDMA (volatility tandem differential mobility analyzer) and H-TDMA (hygroscopic tandem differential mobility analyzer or humidified tandem differential mobility analyzer) technologies conducted by Petzold et al. [52] during the European PartEmis project predicted a coverage of sulfuric acid on ∼100 nm soot particles to be ∼0.8 monolayer coverage for a similar FSC (383 vs 410 ppmm sulfur in the fuel for APEX and PartEmis, respectively). As Petzold et al. [52] points out, they did not have chemical measurements and thus assumed the complete coating was sulfuric acid, thus potentially overestimating the coating thickness of just sulfate if significant organic species were present. The combined sulfate and organic coatings for the low-sulfur fuel cases at high engine power were ∼5.7 mg/kg fuel, or ∼0.3 monolayer coverage. These coatings, especially with respect to the measured sulfate, are less than the coatings measured by Petzold et al. [52] for FSC ∼400 ppmm sulfur and closer to the coatings reported for low-FSC fuel conditions (∼50 ppmm sulfur).

Using the lower limit of particulate sulfate measured during APEX (1.5 mg/kg fuel) and the measured FSC (383 ppmm sulfur), and assuming that all of the particulate sulfate was generated from the fuel sulfur content, the fraction of sulfur that has been converted to particulate sulfate from the fuel sulfur is ∼0.13%. Kärcher et al. observed that fuel sulfur conversion percent estimates ranging from 0.5 to 5% can be used to explain most observations of EI_n and EI_m for sulfate in aircraft exhaust emissions [53]. Recent measurements using chemical ionization mass spectrometry [54–56] indicate that the conversion efficiency is likely greater than 0.34%, and perhaps around 2%, though the measured and modeled results for this important parameter vary widely (0.13% to greater than 30%, where the low value is from this study and a collection of published values are tabulated in Table 8 of Schumann et al., 2002 [20] and plotted in Fig. 1 of Katragkou et al., 2004 [55]). The current estimate, based on chemically speciated measurements, represents the lowest conversion efficiency observed. The current estimate represents a lower limit compared to the literature results, due to uncertainty in AMS transmission (particles >30 nm diameter) and collection efficiencies and the fact that the 30-m probe distance and sampling lines used in the study may not have induced all of the S(VI) to condense. For example, modeling work suggests that the EI_m for sulfate measured during this study is representative of fuel sulfur conversion rates between 1–2%, once all of the microphysical processes are taken into account [44]. The broad range in observed and modeled conversion efficiencies of fuel sulfur to sulfate underscores likely dependences upon engine technology, combustion conditions, and, potentially, sampling techniques that have not yet been identified.

The AMS organic mass spectra measured during APEX for a CFM56 engine were different from previous measurements conducted on an RB-211 engine as part of the NASA EXCAVATE project [17]. As detailed by Boudries et al. [57], the EXCAVATE organic signal was likely due to one or more compounds from an engine oil. This result is not too surprising considering the fact that the EXCAVATE experiment studied a Rolls Royce RB-211 engine and the APEX experiment studied a CFM56 (developed by Snecma, France and GE Aviation, U.S.A.) engine with likely different engine oils. The organic signature during APEX was not as consistent as observed during EXCAVATE, indicating that the source of the organic particulate mass likely came from multiple sources (e.g., engine oils, lube oils, and partially burned fuel species). One specific marker observed in small quantities was identified using the National Institute of Science and Technology mass spectral database as a siloxane. The source for this minor component is not known, though organosilicone compounds are used as antifoam additives in engine lubrication oil.

Perhaps the most intriguing issue with respect to the organic particulate mass is the significant increase in the nucleation/growth mode organic content at low engine powers for low-sulfur fuels. Although this study could not quantitatively measure the organic fraction of the nonrefractory PM at low engine powers, multiple results suggested that organic material dominated the low engine power exhaust particulate matter composition: 1) the AMS observed more organics on the nucleation/growth modes than sulfate, even under high-sulfur fuel conditions (Figs. 9 and 11), 2) the AMS (Fig. 10) measured more (∼factor of 2) sulfate on the soot mode during high engine power for the high-sulfur fuel case compared with the low-fuel sulfur cases, but approximately the same amount of

organics, 3) the AMS (Fig. 10) measured more organic in the nucleation/growth mode for the high-sulfur fuel case compared with the low-fuel sulfur cases, such that either the additional sulfate in the nucleation/growth mode increased particle size, allowing the AMS to sample more of the organic particulate mass, or the condensation of the organic particulate mass is coupled to the amount of condensed sulfate, 4) the EI_n (Figs. 6d and 8d) and the SMPS volume distributions (Figs. 9b and 9d) appeared to measure similar number and mass loadings under low-power conditions for the low- and high-sulfur fuels, but varied significantly for the high engine power conditions, and 5) a lower limit for the fuel sulfur conversion was measured to be ~0.13% at high engine power for the low-sulfur fuel cases and it is unlikely that the sulfur conversion increases by a factor of ~10 as the engine power decreases [58]. Although increased fuel sulfur content appears to have increased the nonrefractory mass of the aircraft exhaust at middle to high engine powers, it did not appear to affect the nonrefractory mass at low engine powers; thus, it is likely that most of the nonrefractory particle mass at low engine powers was composed of organic compounds. This increase in nonrefractory particulate organic matter is likely related to the presence of higher concentrations of VOCs observed in the gas phase at low engine power conditions [23]. The higher levels of emitted gas and particulate organic compounds indicate that the CFM56 engine measured during APEX, similar to essentially all aircraft gas turbine engines, was less efficient at the 4–7% engine thrust levels typically used during aircraft idling and taxiing around an airport.

Conclusions

The exhaust emissions from an in-use commercial aircraft engine were characterized in April 2004 as part of the Aircraft Particle Emissions Experiment (APEX) at NASA Dryden Research Center (Edwards Air Force Base, CA). The test aircraft was a DC-8 equipped with four CFM56-2-C1 engines and was parked on a runway pad during testing. The test matrix included seven different engine throttle levels (varying from ground idle to takeoff, 4–93% of maximum rated thrust), three fuel compositions (base, high-sulfur, and high-aromatic), and three sampling distances behind the inboard, right-side engine (1, 10, and 30 m).

At 1 m behind the engine exit plane, the aircraft exhaust contained only the primary refractory carbon soot particles with trace amounts of organics coating the soot at high engine power, where the coating probably formed during the sampling process. The refractory carbon soot formed a single mode that increased in volume-weighted diameter with engine power. The EI_m and EI_n for refractory carbon soot also increased with engine power and did not depend upon fuel type or probe distance. The refractory carbon soot particles were observed to be fractal and have similar physical properties as diesel and premixed flame soot of the same mobility diameters. The observed range in mobility diameter was much smaller for aircraft soot compared with the larger size ranges generated from diesel and premixed flames (e.g., less fluffy).

When sampling at a downstream distance of 30 m, the farthest downstream measured during APEX, the exhaust contained three particle modes: a nucleation/growth mode, the soot mode, and an accumulation mode. The nucleation/growth mode dominated at low engine powers and consisted of nonrefractory sulfate and organic compounds. The organics were the dominate composition of this mode for typical commercial fuel sulfur levels. The soot mode, including condensed nonrefractory sulfate and organic compounds, dominated the emissions under high engine power conditions. The particulate emissions (refractory and nonrefractory) were minimized under nominal throttle levels of 30–60%.

The aromatic content of the fuel was varied (with little change in the fuel hydrogen content) and resulted in no significant changes in the organic or refractory carbon soot aerosol emissions. The sulfur content of the fuel was varied and produced a significant change in the particulate exhaust emissions. The high-sulfur fuel exhibited a significantly larger number and mass of nonrefractory particulate material in the nucleation/growth mode compared with two other lower-sulfur fuel types. The fuel sulfur to sulfate conversion was estimated to have a lower limit of 0.13% based on the condensed sulfate sampled with a probe at 30 m downstream. The sulfate component in the particulate exhaust was observed to be acidic and the organic species were observed to be composed of a different distribution of species than observed during EXCAVATE. The organic component likely had various sources as the mass spectra changed significantly through the experiments. One minor component identified in the particulate organic emissions was a siloxane compound.

Acknowledgments

The authors thank Chowen Wey (NASA Glenn Research Center) and Phil Whitefield (University of Missouri–Rolla) for the opportunity to participate in the Aircraft Particle Emissions Experiment measurement campaign. We thank Robert Prescott (Aerodyne Research, Inc.) for logistical support; Arnold Engineering Development Center, NASA, University of Missouri–Rolla, and U.S. Environmental Protection Agency crews for sampling probe design, installation, and operation; NASA Dryden Flight Research Center for providing the facilities; and the Aircraft Particle Emissions Experiment team for making the experiment a success. Funding for this project came from the University of Missouri Center of Excellence for Aerospace Particulate Emissions Reduction Research (NASA Cooperative Agreement NCC3-1084) under University of Missouri–Rolla Subcontract No. 000729-02.

References

[1] U.S. Dept. of Transportation, "National Transportation Statistics," 2008, http://www.bts.gov/publications/national_transportation_statistics/.

[2] Pison, I., and Menut, L., "Quantification of the Impact of Aircraft Traffic Emissions on Tropospheric Ozone over Paris Area," *Atmospheric Environment*, Vol. 38, No. 7, 2004, pp. 971–983. doi:10.1016/j.atmosenv.2003.10.056

[3] Yu, K. N., Cheung, Y. P., Cheung, T., and Henry, R. C., "Identifying the Impact of Large Urban Airports on Local Air Quality by Nonparametric Regression," *Atmospheric Environment*, Vol. 38, No. 27, 2004, pp. 4501–4507. doi:10.1016/j.atmosenv.2004.05.034

[4] Spicer, C. W., Holdren, M. W., Riggin, R. M., and Lyon, T. F., "Chemical Composition and Photochemical Reactivity of Exhaust from Aircraft Turbine Engines," *Annales Geophysicae*, Vol. 12, Nos. 10–11, 1994, pp. 944–955. doi:10.1007/s00585-994-0944-0

[5] Unal, A., Hu, Y., Chang, M. E., Talat Odman, M., and Russell, A. G., "Airport Related Emissions and Impacts on Air Quality: Application to the Atlanta International Airport," *Atmospheric Environment*, Vol. 39, No. 32, 2005, pp. 5787–5798. doi:10.1016/j.atmosenv.2005.05.051

[6] Fahey, D. W., Keim, E. R., Boering, K. A., Brock, C. A., Wilson, J. C., Jonsson, H. H. et al., "Emission Measurements of the Concorde Supersonic Aircraft in the Lower Stratosphere," *Science*, Vol. 270, No. 5233, 1995, pp. 70–74. doi:10.1126/science.270.5233.70

[7] Hendricks, J., Kaercher, B., Doepelheuer, A., Feichter, J., Lohmann, U., and Baumgardner, D., "Simulating the Global Atmospheric Black Carbon Cycle: A Revisit to the Contribution of Aircraft Emissions," *Atmospheric Chemistry and Physics*, Vol. 4, 2004, pp. 2521–2541, www.atmos-chem-phys.org/acp/4/2521/.

[8] Schlager, H., Konopka, P., Schulte, P., Schumann, U., Ziereis, H., Arnold, F., Klemm, M., Hagen, D. E., Whitefield, P. D., and Ovarlez, J., "In Situ Observations of Air Traffic Emission Signatures in the North Atlantic Flight Corridor," *Journal of Geophysical Research*, Vol. 102, No. D9, 1997, pp. 10739–10750. doi:10.1029/96JD03748

[9] Colvile, R. N., Hutchinson, E. J., Mindell, J. S., and Warren, R. F., "The Transport Sector as a Source of Air Pollution," *Atmospheric Environment*, Vol. 35, No. 9, 2001, pp. 1537–1565. doi:10.1016/S1352-2310(00)00551-3

[10] Webb, S., "Research Needs Associated with Particulate Emissions at Airports," Airport Cooperative Research Program Rept. 6, 2008.

[11] Penner, J. E., Lister, D. H., Griggs, D. J., Dokken, D. J., and McFarland, M., "Aviation and the Global Atmosphere: A Special Report of the Intergovernmental Panel on Climate Change," 1999, http://

www.grida.no/publications/other/ipcc_sr/?src=/climate/ipcc/aviation/index.htm.

[12] Solomon, S., Qin, D., Manning, M., Alley, R. B., Berntsen, T., Bindoff, N. L. et al., "Technical Summary, Climate Change 2007: The Physical Science Basis. Contribution of Working Group I to the Fourth Assessment Report of the Intergovernmental Panel on Climate Change," 2007, http://www.ipcc.ch/pdf/assessment-report/ar4/wg1/ar4-wg1-ts.pdf.

[13] Jacobson, M. Z., "Strong Radiative Heating Due to the Mixing State of Black Carbon in Atmospheric Aerosols," *Nature*, Vol. 409, No. 6821, 2001, pp. 695–697. doi:10.1038/35055518

[14] Petzold, A., Busen, R., Schroeder, F. P., Baumann, R., Kuhn, M., Stroem, J., Hagen, D. E., Whitefield, P. D., Baumgardner, D., Arnold, F., Borrmann, S., and Schumann, U., "Near-Field Measurements on Contrail Properties from Fuels with Different Sulfur Content," *Journal of Geophysical Research*, Vol. 102, No. D25, 1997, pp. 29,867–29,880. doi:10.1029/97JD02209

[15] Schumann, U., Ström, J., Busen, R., Baumann, R., Gierens, K., Krautstrunk, M., Schröder, F. P., and Stingl, J., "In Situ Observations of Particles in Jet Aircraft Exhausts and Contrails for Different Sulfur-Containing Fuels," *Journal of Geophysical Research*, Vol. 101, No. D3, 1996, pp. 6853–6870. doi:10.1029/95JD03405

[16] Howard, R. P., Hiers, R. S., Jr., Whitefield, P. D., Hagen, D. E., Wormhoudt, J. C., Maike-Lye, R. C., and Strange, R., "Experimental Characterization of Gas Turbine Emissions at Simulated Flight Altitude Conditions," Arnold Engineering Development Center TR-96-3, 1996.

[17] Anderson, B. E., H.-S. Branham, Hudgins, C. H., Plant, J. V., Ballenthin, J. O., Miller, T. M. et al., "Experiment to Characterize Aircraft Volatile Aerosol and Trace-Species Emissions (EXCAVATE)," NASA TM-2005-213783, 2005.

[18] Whitefield, P. D., Hagen, D. E., Wormhoudt, J. C., Miake-Lye, R. C., Wilson, C., Brundish, K., Waitz, I., Lukachko, S., and Yam, C. K., "NASA/QinetiQ Collaborative Program-Final Report," NASA CR-2002-211900, ARL-CR-0508, 2002.

[19] Wilson, C. W., Petzold, A., Nyeki, S., Schumann, U., and Zellner, R., "Measurement and Prediction of Emissions of Aerosols and Gaseous Precursors from Gas Turbine Engines (PartEmis): An Overview," *Aerospace Science and Technology*, Vol. 8, No. 2, 2004, pp. 131–143.

[20] Schumann, U., Arnold, F., Busen, R., Curtius, J., Kärcher, B., Kiendler, A., Petzold, A., Schlager, H., Schröder, F., and Wohlfrom, K. H., "Influence of Fuel Sulfur on the Composition of Aircraft Exhaust Plumes: The Experiments SULFUR 1–7," *Journal of Geophysical Research*, Vol. 107, No. D15, 2002, pp. 4247–4275. doi:10.1029/2001JD000813.

[21] Wey, C. C., Anderson, B. E., Wey, C., Li-Jones, X., Winstead, E., Thornhill, L. K. et al., "Aircraft Particle Emissions Experiment (APEX)," NASA TM-2006-214382, 2006.

[22] Kolb, C. E., Herndon, S. C., McManus, J. B., Shorter, J. H., Zahniser, M. S., Nelson, D. D., Jayne, J. T., Canagaratna, M. R., and Worsnop, D. R., "Mobile Laboratory with Rapid Response Instruments for Real-Time Measurements of Urban and Regional Trace Gas and Particulate Distributions and Emission Source Characteristics," *Environmental Science and Technology*, Vol. 38, No. 21, 2004, pp. 5694–5703. doi:10.1021/es030718p

[23] Knighton, W. B., Rogers, T. M., Anderson, B. E., Herndon, S. C., Yelvington, P. E., and Miake-Lye, R. C., "Quantification of Aircraft Engine Hydrocarbon Emissions Using Proton Transfer Reaction Mass Spectrometry," *Journal of Propulsion and Power*, Vol. 23, No. 5, 2007, pp. 949–958. doi:10.2514/1.22965

[24] Yelvington, P. E., Herndon, S. C., Wormhoudt, J. C., Jayne, J. T., Miake-Lye, R. C., Knighton, W. B., and Wey, C., "Chemical Speciation of Hydrocarbon Emissions from a Commercial Aircraft Engine," *Journal of Propulsion and Power*, Vol. 23, No. 5, 2007, pp. 912–918. doi:10.2514/1.23520

[25] Wormhoudt, J., Herndon, S. C., Yelvington, P. E., Miake-Lye, R. C., and Wey, C., "Nitrogen Oxide (NO/NO2/HONO) Emissions Measurements in Aircraft Exhausts," *Journal of Propulsion and Power*, Vol. 23, No. 5, 2007, pp. 906–911. doi:10.2514/1.23461

[26] Lobo, P., Hagen, D. E., Whitefield, P. D., and Alofs, D. J., "Physical Characterization of Aerosol Emissions from a Commercial Gas Turbine Engine," *Journal of Propulsion and Power*, Vol. 23, No. 5, 2007, p. 919. doi:10.2514/1.26772

[27] Jayne, J. T., Leard, D. C., Zhang, X., Davidovits, P., Smith, K. A., Kolb, C. E., and Worsnop, D. R., "Development of an Aerosol Mass Spectrometer for Size and Composition Analysis of Submicron Particles," *Aerosol Science and Technology*, Vol. 33, Nos. 1–2, 2000, pp. 49–70. doi:10.1080/027868200410840

[28] Canagaratna, M. R., Jayne, J. T., Jimenez, J. L., Allan, J. D., Alfarra, M. R., Zhang, Q. et al. "Chemical and Microphysical Characaterization of Ambient Aerosols with the Aerodyne Aerosol Mass Spectrometer," *Mass Spectrometry Reviews*, Vol. 26, No. 2, 2007, pp. 185–222. doi:10.1002/mas.20115

[29] Jiménez, J. L., Jayne, J. T., Shi, Q., Kolb, C. E., Worsnop, D. R., Yourshaw, I., Seinfeld, J. H., Flagan, R. C., Zhang, X., Smith, K. A., Morris, J., and Davidovits, P., "Ambient Aerosol Sampling Using the Aerodyne Aerosol Mass Spectrometer," *Journal of Geophysical Research*, Vol. 108, No. D7, 2003, p. 8425. doi:10.1029/2001JD001213

[30] Allan, J. D., Jiménez, J. L., Williams, P. I., Alfarra, M. R., Bower, K. N., Jayne, J. T., Coe, H., and Worsnop, D. R., "Quantitative Sampling Using an Aerodyne Aerosol Mass Spectrometer, 1: Techniques of Data Interpretation and Error Analysis," *Journal of Geophysical Research*, Vol. 108, No. D3, 2003, p. 4090. doi:10.1029/2002JD002358

[31] Liu, P. S. K., Deng, R., Smith, K. A., Williams, L. R., Jayne, J. T., Canagaratna, M. R., Moore, K., Onasch, T. B., Worsnop, D. R., and Deshler, T., "Transmission Efficiency of an Aerodynamic Focusing Lens System: Comparison of Model Calculations and Laboratory Measurements for the Aerodyne Aerosol Mass Spectrometer," *Aerosol Science and Technology*, Vol. 41, No. 8, 2007, pp. 721–733. doi:10.1080/02786820701422278

[32] Slowik, J. G., Stainken, K., Davidovits, P., Williams, L. R., Jayne, J. T., Kolb, C. E., Worsnop, D. R., Rudich, Y., DeCarlo, P., and Jiménez, J. L., "Particle Morphology and Density Characterization by Combined Mobility and Aerodynamic Diameter Measurements, Part 2: Application to Combustion Generated Soot Aerosols as a Function of Fuel Equivalence Ratio," *Aerosol Science and Technology*, Vol. 38, No. 12, 2004, pp. 1206–1222. doi:10.1080/027868290903916

[33] Huffman, J. A., Jayne, J. T., Drewnick, F., Aiken, A. C., Onasch, T., Worsnop, D. R., and Jiménez, J. L., "Design, Modeling, Optimization, and Experimental Tests of a Particle Beam Width Probe for the Aerodyne Aerosol Mass Spectrometer," *Aerosol Science and Technology*, Vol. 39, No. 12, 2005, pp. 1143–1163. doi:10.1080/02786820500423782

[34] Petzold, A., Kramer, H., and Schönlinner, M., "Continuous Measurement of Atmospheric Black Carbon Using a Multi-Angle Absorption Photometer," *Environmental Science and Pollution Research International*, Vol. 9, No. 4, 2002, pp. 78–82.

[35] Petzold, A., and Schönlinner, M., "Multi-Angle Absorption Photometry: A New Method for the Measurement of Aerosol Light Absorption and Atmospheric Black Carbon," *Journal of Aerosol Science*, Vol. 35, No. 4, 2004, pp. 421–441. doi:10.1016/j.jaerosci.2003.09.005

[36] Bond, T. C., Anderson, T. L., and Campbell, D., "Calibration and Intercomparison of Filter-Based Measurements of Visible Light Absorption by Aerosols," *Aerosol Science and Technology*, Vol. 30, No. 6, 1999, pp. 582–600. doi:10.1080/027868299304435

[37] DeCarlo, P., Slowik, J. G., Worsnop, D. R., Davidovits, P., and Jiménez, J. L., "Particle Morphology and Density Characterization by Combined Mobility and Aerodynamic Diameter Measurements, Part 1: Theory," *Aerosol Science and Technology*, Vol. 38, No. 12, 2004, pp. 1185–1205. doi:10.1080/027868290903907

[38] Baron, P. A., Sorensen, C. M., and Brockmann, J. E., "Nonspherical Particle Measurements: Shape Factors, Fractals, and Fibers," *Aerosol Measurement: Principles, Techniques, and Applications*, Wiley, New York, 2001.

[39] Hinds, W. C., *Aerosol Technology: Properties, Behavior, and Measurements of Airborne Particles*, Wiley, New York, 1999.

[40] Herndon, S. C., Onasch, T. B., Frank, B., Marr, L. C., Jayne, J. T., Canagaratna, M. R., Lanni, T., Anderson, B. E., Worsnop, D., and Miake-Lye, R. C., "Particulate Emissions from In-Use Commercial Aircraft," *Aerosol Science and Technology*, Vol. 39, No. 8, 2005, pp. 799–809. doi:10.1080/02786820500247363

[41] Moses, C. A., "Aircraft Particle Emissions Experiment (APEX), Appendix B: Fuel Technology Support for NASA Aircraft Particle Emissions Experiment (APEX)," NASA TM-2006-214382, 2006.

[42] Onasch, T. B., Jayne, J., Herndon, S., Mortimer, P., Worsnop, D., and Maike-Lye, R. C., "Aircraft Particle Emissions Experiment (APEX), Appendix J: Chemical Properties of Aircraft Engine Exhaust Aerosols

Sampled during APEX," NASA TM-2006-214382, 2006.
[43] Lobo, P., Hagen, D. E., and Whitefield, P. D., "Aircraft Particle Emissions Experiment (APEX), Appendix I: Physical Characterization of Aerosol Emissions from a Commercial Gas Turbine Engine-Project APEX," NASA TM-2006-214382, 2006.
[44] Wong, H. W., Yelvington, P. E., Timko, M. T., Onasch, T. B., Miake-Lye, R. C., Zhang, J., and Waitz, I. A., "Microphysical Modeling of Ground-Level Aircraft-Emitted Aerosol Formation: Roles of Sulfur-Containing Species," *Journal of Propulsion and Power*, Vol. 24, No. 3, 2008, pp. 590–602. doi:10.2514/1.32293
[45] Davidson, M. J., and Wang, H. J., "Strongly Advected Jet in a Coflow," *Journal of Hydraulic Engineering*, Vol. 128, No. 8, 2002, pp. 742–752. doi:10.1061/(ASCE)0733-9429(2002)128:8(742)
[46] Park, K., Cao, F., Kittelson, D. B., and McMurry, P. H., "Relationship Between Particle Mass and Mobility for Diesel Exhaust Particles," *Environmental Science and Technology*, Vol. 37, No.3, 2003, pp. 577–583. doi:10.1021/es025960v
[47] Laskin, A., Cowen, K. A., Alexander, M. L., Desyaterik, Y., Cowin, J. P., Joseph, D. W., and Spicer, C. W., "Case Study of Particulate Emissions from In-Service C-130 Military Aircraft," *ACS Fuel Chemistry Division Preprint*, Vol. 51, No. 1, 2006, pp. 248–249.
[48] Brown, R. C., Anderson, M. R., Miake-Lye, R. C., Kolb, C. E., Sorokin, A. A., and Buriko, Y. Y., "Aircraft Exhaust Sulfur Emissions," *Geophysical Research Letters*, Vol. 23, No. 24, 1996, pp. 3603–3606. doi:10.1029/96GL03339
[49] Brown, R. C., Miake-Lye, R. C., Anderson, M. R., Kolb, C. E., and Resch, T. J., "Aerosol Dynamics in Near-Field Aircraft Plumes," *Journal of Geophysical Research*, Vol. 101, No. D17, 1996, pp. 22,939–22,954. doi:10.1029/96JD01918
[50] Kärcher, B., Hirschberg, M. M., and Fabian, P., "Small-Scale Chemical Evolution of Aircraft Exhaust Species at Cruising Altitudes," *Journal of Geophysical Research*, Vol. 101, No. D10, 1996, pp. 15169–15190. doi:10.1029/96JD01059
[51] Jayne, J. T., Pöschl, U., Chen, Y.-M., Dai, D., Molina, L. T., Worsnop, D. R., Kolb, C. E., and Molina, M. J., "Pressure and Temperature Dependence of the Gas-Phase Reaction of SO3 with H2O and the Heterogeneous Reaction of SO3 with H2O/H2SO4 Surfaces," *Journal of Physical Chemistry A: Molecules, spectroscopy, kinetics, environment, & general theory*, Vol. 101, No. 51, 1997, pp. 10000–10011. doi:10.1021/jp972549z
[52] Petzold, A., Gysel, M., Vancassel, X., Hitzenberger, R., Puxbaum, H., Vrochticky, S., Weingartner, E., Baltensperger, U., and Mirabel, P., "On the effects of organic matter and sulphur-containing compounds on the CCN activation of combustion particles," *Atmospheric Chemistry and Physics*, Vol. 5, 2005, pp. 3187–3203, www.atmos-chem-phys.org/acp/5/3187/.
[53] Kärcher, B., Turco, R. P., Yu, F., Danilin, M. Y., Weisenstein, D. K., Miake-Lye, R. C., and Busen, R., "A unified model for ultrafine aircraft particle emissions," *Journal of Geophysical Research*, Vol. 105, No. D24, 2000, pp. 29379–29386.
[54] Curtius, J., Sierau, B., Arnold, F., Baumann, R., Busen, R., Schulte, P., and Schumann, U., "First direct sulfuric acid detection in the exhaust plume of a jet aircraft in flight," *Geophysical Research Letters*, Vol. 25, No. 6, 1998, pp. 923–926. doi:10.1029/98GL00512
[55] Katragkou, E., Wilhelm, S., Arnold, F., and Wilson, C., "First Gaseous Sulfur (VI) Measurements in the Simulated Internal Flow of an Aircraft Gas Turbine Engine During Project PartEmis," *Geophysical Research Letters*, Vol. 31, No.2, 2004, pp. L02117. doi:10.1029/2003GL018231
[56] Sorokin, A., Katragkou, E., Arnold, F., Busen, R., and Schumann, U., "Gaseous SO3 and H2SO4 in the Exhaust of an Aircraft Gas Turbine Engine: Measurements by CIMS and Implications for Fuel Sulfur Conversion to Sulfur (VI) and Conversion of SO3 to H2SO4," *Atmospheric Environment*, Vol. 38, No. 3, 2004, pp. 449–456. doi:10.1016/j.atmosenv.2003.09.069
[57] Boudries, H., Canagaratna, M., Onasch, T., Worsnop, D., Wormhoudt, J., Miake-Lye, R., and Anderson, B., "Experiment to Characterize Aircraft Volatile Aerosol and Trace-Species Emissions (EXCAVATE), Appendix F: Real Time Characterization of Aircraft Particulate Emission by an Aerosol Mass Spectrometer During EXCAVATE 2002," NASA TM-2005-213783, 2005.
[58] Lukachko, S. P., Waitz, I. A., Miake-Lye, R. C., and Brown, R. C., "Engine Design and Operational Impacts on Particulate Matter Precursor Emissions," *Journal of Engineering for Gas Turbines and Power*, Vol. 130, No. 2, 2008, p. 021505. doi:10.1115/1.2795758.

L. Maurice
Associate Editor